공학박사 학위논문

Methane activation at low temperature in the presence of oxygen using plasma-catalyst hybrid system

산소 조건에서 플라즈마-촉매 하이브리드 시스템을 이용한 저온에서의 메탄활성화 반응

2018년 2월

서울대학교 대학원

화학생물공학부

이 희 수

Abstract

Methane activation at low temperature in the presence of oxygen using plasma-catalyst hybrid system

Heesoo Lee
School of Chemical and Biological Engineering
The Graduate School
Seoul National University

Natural gas is one of the most abundant fossil fuels around the world. Cleaner energy source than other fossil fuels and world-wide presence of natural gas make it an attractive energy source. Despite of these advantages, the emission of unburned natural gas makes it difficult to use since the methane is recognized as the major portion of global warming gas. It contributes 25–34 times more to global warming than CO_2 at equivalent emission rate and has quite long lifetime. Therefore, complete oxidation of methane is one of the critical problems to solve for widening the use of methane without worrying about the environmental concern such as global warming. Except for the role as fuel, the utilization of methane has been limited mostly to the route of synthesis gases to produce liquid hydrocarbons and other chemical products, which is regarded as indirect methods. Such indirect process has weaknesses of high operating cost and low

thermodynamic efficiency due to the swing between endothermic and exothermic reaction. Hence, if methane is directly utilized as alternate feedstock to petroleum, it will be highly desirable from the economic point of view. Thus, many efforts have been made for the direct conversion of methane into more useful products like olefins, aromatics, and alcohols by using various catalysts for decades. However, harsh reaction conditions including high temperature and pressure are required to start the catalytic reaction such as complete oxidation of methane and direct conversion of methane to value-added chemicals because methane can be hardly activated due to its stable C-H bond. The methane activation is the key step to initiate such reactions. In order to overcome these difficulties, various catalysts were investigated and applied. Nevertheless, the activation of methane is still hard to be carried out because tough reaction condition can deactivate the catalyst. An alternative way to activate methane at low temperature would be to use plasma. There are various thermal and non-thermal plasma sources such as dielectric barrier discharge (DBD), corona, gliding arc, rotating arc, spark, microwave, glow discharge and pulsed discharge. In the non-thermal plasma, high-energy electrons (1-20 eV) are produced and they can initiate the formation of other various radicals. Since electron mass is very light, non-thermal plasma gives rise to the increase in temperature by only few degrees. In this work, dielectric barrier discharge (DBD) plasma was used since it is easier to set up than other non-thermal plasma sources.

Firstly, the complete oxidation of methane was carried out in a dielectric barrier discharge (DBD) quartz tube reactor where both catalyst and plasma were hybridized into one in-plasma catalysis system. Non-PGM catalysts such as $Co_1Ni_1O_x$ and $CoCr_2O_4$ were used as oxidation catalyst. Input voltage of the plasma-catalyst reactor maintained to $4kV_{p-p}$ to minimize the effect of plasma

power for plasma-catalyst interaction. In the absence of catalyst, methane began to be oxidized to CO and CO_2 even at room temperature, and the conversion increased with the increment of temperature since the active radicals were generated more abundantly under those conditions. However, large amount of CO were also produced in addition to CO_2, especially at low temperature below 200 °C when plasma was only used. In the presence of both plasma and catalyst, however, methane was oxidized even at room temperature mostly to CO_2 with low CO selectivity over certain non-PGM catalyst like $Co_1Ni_1O_x$, indicating that the complete oxidation was successfully performed with the aid of catalyst. The role of plasma was to oxidize CH_4 to produce CO, which was subsequently oxidized to CO_2 over catalyst at low temperature. Hence, methane complete oxidation reaction proceeded at much lower temperature similar to PGM catalyst such as Pd/Al_2O_3, while maintaining low CO selectivity.

Next, oxidative coupling of methane (OCM) was carried out to produce C_2 or C_3 hydrocarbons from methane under plasma-catalyst hybrid system. Dielectric barrier discharge (DBD) plasma was applied as plasma source to lower the reaction temperature since catalyst only reaction required high temperature above 700 ºC. Plasma only reaction was performed to compare with plasma-catalyst hybrid reaction. We tried to seek appropriate support under plasma-catalyst hybrid reaction at low temperature. Among various supports, only SiO_2 has shown the higher yield when combined with dielectric barrier discharge plasma than plasma only reaction. When various metals were impregnated on SiO_2 to investigate the effect under plasma condition, it was found that Ag/SiO_2 demonstrated the highest C_{2+} hydrocarbon yield of about 10% below the reaction temperature of 400 ºC. In

this process, oxygen was proved to play an essential role in the coupling of methane to C_{2+} hydrocarbons over Ag/SiO_2 catalyst. However, Ag/SiO_2 catalyst under plasma condition became deactivated with time-on-stream because of coking. However, during the stability test with time-on-stream, Ag/SiO_2 catalyst with plasma became deactivated due to coking. Therefore, regeneration process was introduced after OCM reaction. As a result, it was found that plasma regeneration at 378 °C gave rise to the full recovery of activity while thermal regeneration did not due to partial removal of coke and sintering of Ag.

Finally, the direct methanol synthesis from methane was carried out in a plasma-catalyst hybrid system. Since catalyst only reaction requires high pressure and batch reactor, dielectric barrier discharge (DBD) plasma was applied as a plasma source to overcome the difficulties. Among the transition metal oxides, Mn_2O_3-coated glass bead showed the highest methanol yield about 12.3% in the plasma-catalyst hybrid system. The reaction temperature was maintained below 100 ºC because of low plasma input power (from 1.3 kJ/L to 4.5 kJ/L). Furthermore, the reactivity of the catalyst was maintained for 10 h without changing the selectivity. The mechanistic study indicated that the plasma-induced OH radical generated on the transition metal oxide catalyst possessed high selectivity toward methane to produce methanol.

Keywords: Methane activation, plasma-catalyst hybrid system, dielectric barrier discharge, low temperature reaction

Student Number: 2014-30264

Contents

List of Scheme and Tables

List of Figures

Chapter 1. Introduction

The utilization of fossil fuels such as coal, petroleum, and natural gas has produced large amount of energy. However, most of useful chemicals are manufactured from the petroleum. For a long period of time, natural gas have been much cheaper than petroleum [1]. Natural gas of which major component is methane is widely distributed all over the world [2]. The world-wide presence of natural gas and the fact that natural gas is regarded as clean energy source compared to other fossil fuels make it an attractive alternative energy source. Besides this, natural gas has potential technical and economic advantages due to achievable high fuel efficiencies and attractive cost, respectively [3]. Despite of these advantages, the emission of unburned natural gas makes it difficult to use since the methane is recognized as the major portion of global warming gas. Therefore, treatment of residual natural gas is one of the critical problems to solve for widening the use of methane without worrying about the environmental concern such as global warming. The utilization of natural gas is limited to mostly fuel or synthesis gases to produce liquid hydrocarbons and other chemical products by indirect methods [4, 5]. These indirect processes have weaknesses of longer time and higher cost for operation. In this circumstance, if natural gas is directly utilized as alternate feedstock to petroleum, it will be highly desirable for industrial catalysis reaction. Hence, many efforts have been performed for direct methane conversion into more useful products like olefins and aromatics for decades using various catalysts [6-10]. In order to deal with the methane emission and to convert the methane into useful products, the methane should be activated first.

1.1. Methane

Methane is the simplest alkane which has chemical formula CH_4. It is the main constituent of natural gas and its abundance on Earth makes it an attractive fuel. However, capturing and storing it are regarded as challenge due to its gaseous state under normal conditions of temperature and pressure. Methane is a tetrahedral molecule with four equivalent C-H bonds. C-H bond of the methane is stable because of high bond energy (413 kJ/mol) [11]. The primary chemical reactions of methane are combustion, steam reforming to synthesis gas, and halogenation [12-14]. In general, methane reactions are difficult to start and control due to the stable structure of it.

1.2. Plasma

Plasma is one of the four fundamental states of matter, which was first introduced by chemist Irving Langmuir in the 1920s [15]. Plasma can simply be considered as a gaseous mixture of negatively charged electrons and highly charged positive ions. The overall charge of the plasma is roughly zero. Plasma production is from the distinct separation of these ions and electrons that produces electric field, which in turn, produces electric currents and magnetic fields. Unlike the other three states of solid, liquid, and gas, plasma does not freely exist in the Earth under normal surface conditions, and can only be artificially generated by heating neutral gases or by subjecting that gas into a strong electromagnetic field [16]. Plasma can be divided into thermal and non-thermal plasma. There are various thermal and non-thermal plasma sources such as dielectric barrier discharge (DBD), corona, gliding arc, rotating arc, spark, microwave, glow discharge and pulsed discharge with catalyst or without catalyst [17, 18].

1.2.1. Thermal Plasma

In the case of thermal plasma, a state of local thermodynamic equilibrium is approached. Therefore, the temperature of electrons and bulk gas becomes almost same. Thermal plasma have numerous advantages including high temperature, high intensity, non-ionizing radiation, and high-energy density. Due to high mobility of atoms, molecules, ions, and electrons the energy applied to plasma is captured by electrons and transferred to heavy particles via elastic collision. Because of high electron number density, elastic collision frequencies are very high, which leads to the rapid thermal equilibrium. The heat source is also directional with sharp interfaces and sheer thermal gradients that can be controlled independently of

chemistry. While burning fossil fuels can hardly achieve temperature over 2000 °C while the electrically generated thermal plasma can reach temperature of 20000 °C or more [19]. Thermal plasma technologies are used for a various applications involving coating techniques, fine powder synthesis, metallurgy, and treatment of hazardous waste materials. However, thermal plasma is not appropriate to use with catalyst because high temperature of the plasma can destruct or deactivate the catalyst.

1.2.2. Non-thermal plasma

In general, non-thermal plasma is the plasma that is not in thermodynamic equilibrium because the ion temperature is different from the electron temperature. In the non-thermal plasma condition, thermal motion of the ions can be neglected. This leads to the fact that there is no pressure force and the magnetic force can be ignored. Consequently, only the electric force is considered to act on the particles. High-energy electrons (1-20 eV) are produced and they can initiate the formation of other various radicals. Because electron mass is very light, non-thermal plasma gives rise to the increase in temperature by only few degrees [20]. Hence, non-thermal plasma is also referred to as “cold plasma” or “non-equilibrium plasma” [21]. As such, partially ionized gas can be created using simple reactor configuration and relatively inexpensive power source, while almost isothermal reaction condition is maintained. This plasma is used for the applications like local surface modification or surface activation because the ions, atoms, and molecules remain relatively cold and do not cause thermal damage to the surface. This property enables it to be utilized for low temperature chemistry, plasma etching, deposition, surface modification, and treatment of heat sensitive materials. Various

non-thermal plasma sources are currently being used for combining with catalytic system since non-thermal plasma scarcely influence the catalyst. Among those, DBD requires alternating voltage and at least one dielectric barrier between high voltage electrode and ground electrode [22]. Because of the dielectric barrier, the DBD is a non-equilibrium discharge, which means that high temperature electrons are created in the micro-discharges. They can initiate plasma-induced chemical reactions without increasing the temperature substantially.

1.3. Plasma-catalyst hybrid system

Plasma and catalyst have their own advantages and disadvantages. The catalyst is highly selective while it is active only at high temperature since reactants must overcome the activation energy. On the other hand, the plasma can be highly reactive even at room temperature although it is nonselective. Hence, the hybridization of plasma and catalyst into one system can provide complementary or even synergistic results for the reactant activation at low temperature [23]. Previous studies have shown the positive effect of using a plasma-catalyst combination system on various reactions such as oxidation, dissociation, reduction, and reforming [24-28]. Heterogeneous catalyst can be combined with non-thermal plasma in two ways: the catalyst in the discharge zone (in-plasma catalysis, IPC) or the catalyst after the discharge zone (post-plasma catalysis, PPC) as shown in Figure 1-1. Catalyst can be put into a reactor as a packed bed in several ways, such as a layer of catalyst material or coating on the reactor wall or electrodes [29]. In order to maximize an influence of short-lived radical on catalytic reactions, it is desirable for plasma to take place near the catalyst surface. Hence, IPC hybrid system was applied in this study.

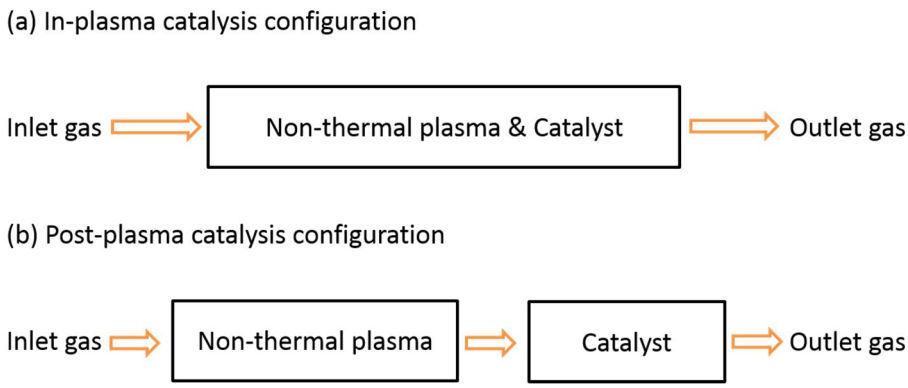

Figure 1-1. Schematic overview of two plasma-catalyst hybrid system configurations; (a) in-plasma catalysis (IPC) and (b) post-plasma catalysis (PPC).

1.4. Voltage-charge Lissajous method

According to the gas discharge theory, the load characteristics of a reactor are equivalent to that of a capacitor, and the DBD process is equal to the charge and discharge transitions of the capacitor [30, 31]. The capacitor was placed between the ground electrode of the reactor and the ground to examine the transported charges. According to the equations (1) and (2) in the following, the plasma power can be obtained by measuring the area of the V-Q Lissajous cyclogram. The slope of discharge transitions is equal to dielectric capacitance, and that of capacitive transitions is equal to the total capacitance of the discharge reactor [30].

$$P = \frac{1}{T}\int_0^T U(t)I(t)dt = \frac{1}{T}\oint U(Q)dQ = C_M f \oint U(U_C)dU_C = f \cdot S \qquad (1)$$

$$\text{Specific input energy}(J/L) = \frac{P\ (W)}{\text{gas flow rate}(L/s)} \qquad (2)$$

Where P = discharge power, T = time, I = current, U = voltage, Q = charge, C_M = measuring capacitor, U_C = voltage of measuring capacitor, f = frequency, S = area of Lissajous figure.

1.5. Objectives

Although the methane activation reaction has been studied for decades, the methane activation reaction using plasma-catalyst hybrid system was rarely investigated. This thesis mainly consists of studying the synergistic effect between plasma and catalyst on the methane activation reaction in order to suggest appropriate catalyst and optimum plasma condition for the treatment of methane and selective production of value-added chemicals directly from methane. Plasma only reaction is investigated first in order to establish a reference for plasma-catalyst hybrid reaction. The plasma only reaction is helpful for understanding the effect of plasma on the methane activation reaction. Based on the results of plasma only reaction, various supports and catalysts are introduced with the purpose of selectively producing the target chemicals such as carbon dioxide, ethane, ethylene, propane, propylene, and methanol.

Chapter 2. Complementary effect of plasma-catalyst hybrid system on methane complete oxidation over non-PGM catalysts

2.1. Introduction

Natural gas and shale gas are attracting public attention because of its widespread reserves and cleanness compared to other fossil fuels. Nowadays, it is used as a fuel of combined heat power (CHP) and natural gas vehicles (NGV) [32]. However, methane, which is the main component of natural gas, is hard to be burned completely. Such unburned methane is the second most important anthropogenic greenhouse gas in the atmosphere after CO_2 [33]. Shine et al. [34] reported that methane possesses about 25–34 times more global warming potential than CO_2 at equivalent emission volume. Thus, in order to solve this problem, non-PGM catalysts [35-40] as well as noble metal catalysts especially like palladium-based catalysts [41-45] have been employed. However, methane activation at low temperature (i.e. below 200 °C) is still difficult to implement compared to other exhaust gases such as CO, NO_x, or hydrocarbons. Therefore, the combination of plasma and catalyst is currently attracting attention as a method of supplementing the catalysts [46]. Plasma is a partially or fully ionized gas phase composed of various particles like electrons, ions, atoms, and molecules [21]. Various thermal and non-thermal plasma sources, including dielectric barrier discharge (DBD), corona, arc, spark, microwave, and glow discharge have been studied [18, 47]. Plasma can divide into thermal and non-thermal plasma depending on plasma temperature [17]. Thermal plasma is in a phase where almost all components are at thermal equilibrium. Therefore, high temperature (>10,000 K) thermal energy is

generated all over the plasma zone. On the other hand, in non-thermal plasma, the electrons can attain high energy of 1 – 10 eV (10,000-100,000 K) and activate other various molecules while the gas temperature can remain as low as ambient temperature [48]. Thus, temperature is not in thermal equilibrium and it quite differs between the electrons and the other particles like ions, atoms, and molecules [20]. Generally, dielectric barrier discharge (DBD) was selected for realizing the non-thermal plasma.

Plasma and catalyst possess their merits and demerits. The catalyst possesses high selectivity while it needs high thermal energy to activate. On the other hand, the plasma can be reactive even at room temperature whereas it is nonselective and crashes the molecules randomly. Hence, the hybridization of plasma and catalyst into one system is expected to offer complementary or even synergistic effect on the catalytic reaction as the past researchers reported [29, 49]. Herein, the plasma-catalyst hybrid system was applied to observe such effects between plasma and catalyst for methane complete oxidation. According to our previous work [50], palladium-based catalyst under specific condition showed synergistic effect with dielectric barrier discharge (DBD). In this paper, the less expensive non-PGM catalysts such as $CoCr_2O_4$ and $Co_1Ni_1O_x$ were used to investigate the hybridization effect of dielectric barrier discharge (DBD) and non-PGM catalyst on methane complete oxidation.

2.2. Experimental

2.2.1. Reaction system

A schematic view of plasma-catalyst system and equivalent circuit of DBD reaction system are presented in Figure 2-1(a) and 2-1(b), respectively. It consisted of a 1000:1 high voltage probe (Tektronics P6015A), a current probe (Pearson electronics 6585), and a capacitor (1000 pF) for measuring voltage (V), current (A), and transferred electric charge (Q), respectively. All output signals were transmitted to a 100MHz digital oscilloscope (Tektronics DPO 2014) which was utilized to calculate discharge power by the V-Q Lissajous figure method [30, 51].

The catalysts in bead form (Φ=425-600μm) were placed on the quartz filter at the middle of reactor, inside the plasma discharge zone. The height of catalyst bed varied from 5mm to 7mm since the weight of catalyst was 0.5g while their density differed from each other. The catalyst bed temperature was measured and recorded using K type thermocouple which was protected by another quartz tube just below the filter in the reactor. Another thermocouple in the furnace was used to control the setting temperature.

The DBD reactor was made of a quartz tube with an inner diameter of 10mm a thickness of 1.3mm and a length of 500mm. The filter was located at the middle of reactor and its thickness was 2.5mm. In the DBD reactor, catalyst zone and plasma zone were combined at same position to minimize the recombination of active radicals produced by the plasma before reacting at the catalyst surface. Electrical discharge of the reactor was DBD. It consisted of a stainless steel rod of which thickness was 3mm. The rod was centered in a quartz tube reactor, fixed with a groove at the filter and Teflon ferrule. The outer surface of the reactor was surrounded by copper foil with a length of 22 mm and a thickness of 0.05mm. The

length of discharge zone was 22 mm, and the gap was 5 mm, resulting in the reaction volume of about 1.7 cm^3. To create the discharge, an AC high voltage was generated with a maximum of $4kV_{p-p}$ by arbitrary function generator (GW INSTEK AFG-2012) and amplified by high voltage amplifier (TREK 20/20C-HS) with a maximum peak voltage of 20kV and a variable frequency up to 20 kHz. All experiments were carried out under identical conditions of waveform (sinusoid), driving frequency (4 kHz), and applied voltage (4 kV_{p-p}). The atmospheric pressure was maintained in the same quartz reactor.

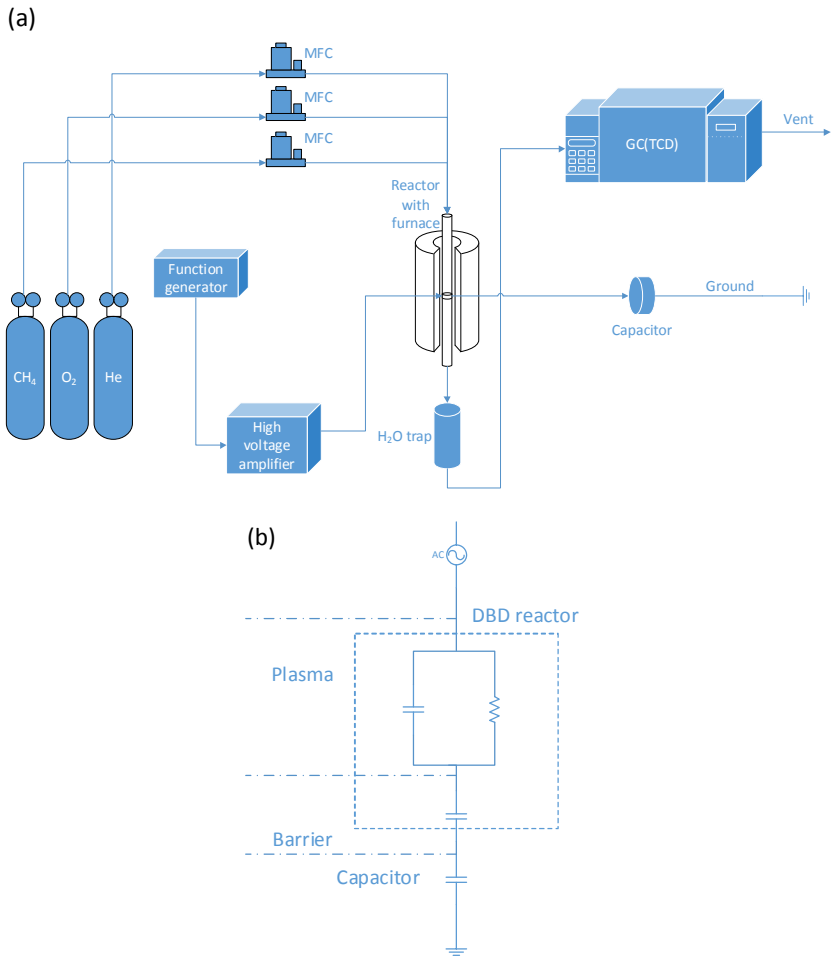

Figure 2-1. (a) Schematic view of plasma-catalyst system and (b) Equivalent circuit of DBD reaction system.

2.2.2. Preparation of catalysts

The Co/Cr mixed oxides catalyst was prepared by a coprecipitation method following the procedure in the reference [52]. A diluted aqueous ammonia (30-33%) solution (Sigma-Aldrich) was added drop by drop to a mixed aqueous solution of chromium nitrate nonahydrate (Sigma-Aldrich) and cobalt nitrate hexahydrate (Sigma-Aldrich) with continuous stirring at 60 °C until the pH value reached 9.1±0.2. The precipitates were filtered, washed several times and dried in an oven at 105 °C overnight. Finally, the dried materials were calcined at 500 °C for 3 h. The Co/Ni mixed oxides catalysts were also prepared by a coprecipitation method. The solution of sodium carbonate (Alfar Aesar) was dropped to a mixed aqueous solution of cobalt nitrate hexahydrate (Sigma-Aldrich) and nickel nitrate hexahydrate (Alfar Aesar) with continuous stirring at 60 °C until the pH value reached 9.1±0.2. The precipitates were filtered, washed several times and dried in an oven at 105 °C overnight. Finally, the dried materials were calcined at 500 °C, 600 °C, 700 °C for 3 h which were named as $Co_1Ni_1O_x$(500), $Co_1Ni_1O_x$(600), $Co_1Ni_1O_x$(700), respectively. The catalysts were sieved to the particle size of 425-600 μm. Solid-state phases was identified with XRD (RIGAKU SMARTLAB) with a Cu Kα radiation operated at 40 kV and 50 mA. Specific surface area of catalysts was also determined by the BET method using ASAP 2010 instrument (Micromeritics Co.).

2.2.3. Activity measurement

The catalytic activity was measured at atmospheric pressure in the same quartz reactor. The reactants were 2500 ppm CH_4, 2.5% O_2, balanced in He. The total gas flow was maintained to 200 ml/min. Each gas mixture was controlled by using

mass flow controllers (SIERRA). Outflow gases passing through the discharge region were analyzed by gas chromatography (AGILENT GC 6890N) equipped with a thermal conductivity detector (TCD) and a 60/80 Carboxen-1000 packed column, which allowed us to measure H_2, O_2, N_2, CO, CO_2, CH_4, C_2H_4, C_2H_6 and C_2H_2. Methane conversion was examined at steady-state condition in the presence and in the absence of catalyst, while increasing the temperature from room temperature to 400 °C by 50 or 100 °C. Methane conversion and selectivity of CH_4, CO, and CO_2 species are defined as:

$$\text{Conversion}(CH_4) = \frac{mol(consumed\ CH_4)}{mol(introduced\ CH_4)} \times 100[\%] \qquad (3)$$

$$\text{Selectivity}(\text{CO}) = \frac{mol(produced\ CO)}{mol(converted\ CH_4)} \times 100[\%] \qquad (4)$$

$$\text{Selectivity}(CO_2) = \frac{mol(produced\ CO_2)}{mol(converted\ CH_4)} \times 100[\%] \qquad (5)$$

2.3. Results and discussion

2.3.1. Textural properties of catalysts

XRD analysis was performed to investigate the crystalline structures of the catalysts. The powder X-ray diffraction patterns for the calcined $CoCr_2O_4$ and $Co_1Ni_1O_x$ catalysts are shown in Figure 2-2. As shown in Figure 2-2(A), XRD patterns of $CoCr_2O_4$ catalyst showed well resolved peaks characteristic of cubic spinel structure and matches well with the reference data (JCPDS 22-1084).

All $Co_1Ni_1O_x$ catalysts exhibited Co_3O_4 (JCPDS 42-1467), $NiCo_2O_4$ (JCPDS 20-0781), and NiO (JCPDS 47-1049) phases. Since Co_3O_4 and $NiCo_2O_4$ had same spinel structure with similar lattice parameter (Co_3O_4 : 8.084 Å, $NiCo_2O_4$: 8.110 Å), the detailed analysis of the XRD pattern in the region of the main peak was performed, as indicated by the right box of Figure 2-2(B). At first, the $Co_1Ni_1O_x$(500) contained $NiCo_2O_4$ phase and NiO phase. However, as the calcination temperature increased, the spinel phase decomposed to form Co_3O_4 and NiO, thus the peak at 36.8° was slightly shifted from that of $NiCo_2O_4$ to that of Co_3O_4. Also, the crystalline size of the catalysts increased sharply with increasing calcination temperature. $Co_1Ni_1O_x$ catalysts peaks observed at 2θ = 36.8° and 43.5° can be assigned to the $NiCo_2O_4$ (311), and NiO (200) phases, respectively. $NiCo_2O_4$ peaks of $Co_1Ni_1O_x$(600) and $Co_1Ni_1O_x$(700) split into two peaks, assigned to Co_3O_4 and NiO phases. Note that the crystalline size of the NiO became bigger as evidenced by the sharpened NiO (111) peak. Also, $NiCo_2O_4$ (311) peak positions were changed to Co_3O_4 (311) as the calcination temperature increased. Such change in peak positions originated from the thermal decomposition of $NiCo_2O_4$ into Co_3O_4 and NiO in $Co_1Ni_1O_x$ sample at elevated temperature.

Table 2-1 lists the specific surface area of all prepared catalysts. $CoCr_2O_4$ had the

surface area of 88 m^2/g, which is the largest value of all catalysts. Surface area of $Co_1Ni_1O_x$ decreased as calcination temperature increased. This was also consistent with XRD results that the crystalline size of the phases in the catalysts were sharply increased which led to decline of specific surface area with increasing calcination temperature.

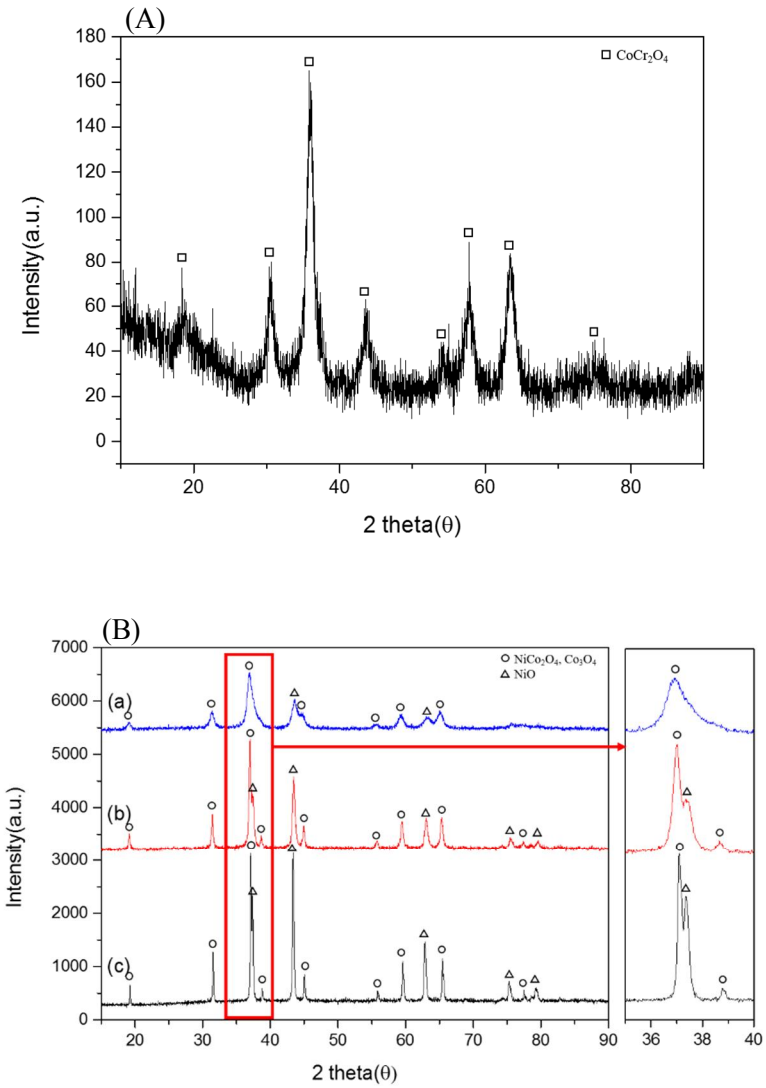

Figure 2-2. XRD patterns of $CoCr_2O_4$ catalyst (A) and $Co_1Ni_1O_x$ catalysts (B) with different calcination temperature; (a) 500°C, (b) 600°C, (c) 700°C.

Table 2-1. Specific surface area of the catalysts

Catalyst	Specific surface area(m^2/g)
$CoCr_2O_4$	88
$Co_1Ni_1O_x$(500)	37
$Co_1Ni_1O_x$(600)	27
$Co_1Ni_1O_x$(700)	6

2.3.2. Methane oxidation reaction under plasma only or catalyst only condition

Firstly, the methane conversion over various non-PGM catalysts in the absence of plasma in addition to one under plasma only condition is shown in Figure 2-3 and Table 2-2. In the absence of plasma, all catalysts started to be activated above 200°C as indicated in light-off temperature of Table 2-2. $CoCr_2O_4$ showed the best performance among them. $Co_1Ni_1O_x$ catalysts exhibited poor activity as the calcination temperature increased. This is due to the decrease of specific surface area and the collapse of spinel structure as demonstrated in XRD pattern. In catalyst only condition, complete oxidation of methane occurred, since CO_2 was only detectable product. Current results over these catalysts have similar activity to that previously reported in the literature for methane complete oxidation [52-56].

Meanwhile, the methane oxidation reaction was carried out under plasma only condition to compare the reaction of plasma and that of catalyst. As summarized in Table 2-2, plasma only condition gave rise to the lowest T_{50} (202 °C), where CO selectivity (47%) was extremely high. The CO selectivity decreased dramatically to 1% with increasing the temperature (T_{90}) to 410 °C, implying that the plasma required enough thermal energy to oxidize CO to CO_2. It can be summarized that non-PGM oxide catalyst requires high temperature (or thermal energy) to completely oxidize methane, while plasma only condition demonstrates the high methane conversion with high CO selectivity at low temperature.

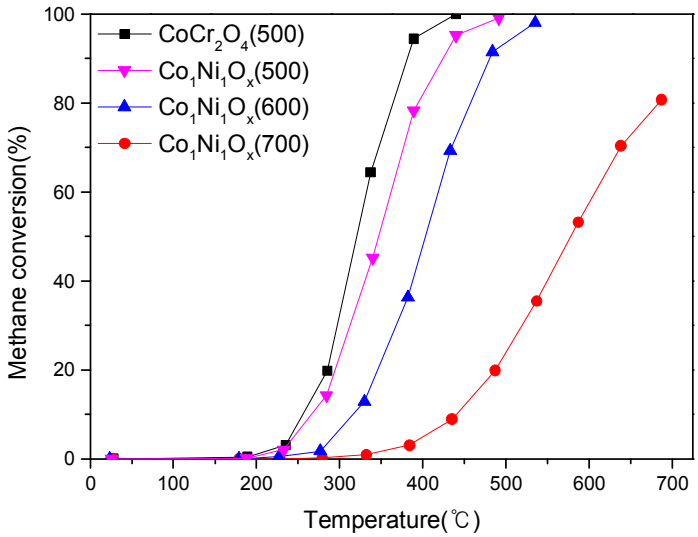

Figure 2-3. Light-off curves of CH_4 oxidation over non-PGM catalysts as a function of temperature in the absence of plasma.

Table 2-2. Light-off temperature of methane oxidation over plasma only and catalyst only system

Condition		Light-off temperature(°C)		
		T_{10}	T_{50}	T_{90}
Catalyst only	$CoCr_2O_4$	255	312	359
	$Co_1Ni_1O_x$(500)	261	351	407
	$Co_1Ni_1O_x$(600)	318	401	478
	$Co_1Ni_1O_x$(700)	440	579	-
Plasma only (CO selectivity(%))*		-	202(47)	410(1)

*CO selectivity is defined as

$$\textbf{Selectivity}\ (\boldsymbol{CO}) = \frac{\boldsymbol{mole\ (produced\ CO)}}{\boldsymbol{mole\ (converted\ CH_4)}} \times \mathbf{100}\ [\%].$$

2.3.3. Methane oxidation under plasma-catalyst hybrid condition

The catalysts were placed inside the discharge zone of plasma to inspect the plasma-catalyst hybridization effect. This hybridization concept was based on other previous plasma-catalyst hybrid applications [57-61]. Especially, the former result [50] indicated the synergistic effect between DBD plasma and palladium-based catalysts. It was found that the combination of plasma and catalyst showed better reactivity and selectivity than catalyst only or plasma only.

Methane conversions on plasma-catalyst hybrid system and plasma only condition are shown in Figure 2-4(a) as a function of temperature. Unlike the catalyst only reactions (Figure 2-3), all oxidation reactions began at room temperature under the hybrid condition. As shown above, catalytic performance of $CoCr_2O_4$ was the highest among any other catalysts in this research. When DBD plasma was applied, however, the circumstance was reversed. At low temperature, plasma dominantly influences the activity so that plasma only reaction showed the highest methane conversion. All catalysts presented somewhat antagonistic effect on methane oxidation under DBD plasma condition. Among them, $CoCr_2O_4$ had the most significant antagonistic result and $Co_1Ni_1O_x$ showed similar effects which was better than that of $CoCr_2O_4$ regardless of the calcination temperature. This was also confirmed in Figure 2-5 indicating that current peaks were getting smaller in the order of plasma only>$Co_1Ni_1O_x$>$CoCr_2O_4$. Accordingly, the specific input energy decreased 186 J/L>168 J/L>162 J/L. This meant plasma generation could be interrupted by the packing material like catalyst in this case. Above about 250 °C, catalysts were activated, thus the order of methane conversion was reversed again. At high temperature, catalyst with high catalytic performance showed high methane conversion in the hybrid system.

Only methane conversion cannot provide the sufficient information to evaluate the plasma-catalyst hybrid system, since CH_4 can be converted to either CO or CO_2. Hence, the CO selectivity result of hybrid reactions is shown in Figure 2-4(b). As described in Table 2-2 and Figure 2-4(b), the CO selectivity increased to about 50% in the absence of the catalyst. The selectivity results were varied depending on the loaded catalyst. The $Co_1Ni_1O_x$(500) catalyst had the lowest CO selectivity while the $CoCr_2O_4$ showed the highest CO selectivity. The CO selectivity of $Co_1Ni_1O_x$ catalysts was significantly enhanced when the calcination temperature was above 700°C. According to the chemical equation in the previous literature [50], CO_2 formation could be affected by the reaction of CH_4 oxidation or CO oxidation. Therefore, this should be checked by examining the CO oxidation ability of the catalysts. Figure 2-6 presents the CO oxidation ability over the catalysts, which explained how the CO selectivity was determined under plasma-catalyst hybrid system. $CoCr_2O_4$ catalyst with the highest methane conversion and the lowest CO conversion had the highest CO selectivity when combined with the plasma. Also, $Co_1Ni_1O_x$(700) catalyst which showed the lower CO conversion presented the higher CO selectivity than other $Co_1Ni_1O_x$ catalysts. In this sense, it was confirmed that the CO selectivity of plasma-catalyst hybrid reaction was not governed by methane oxidation ability but also by CO oxidation ability of each catalysts. Therefore, it can be concluded that plasma play a main role in oxidizing CH_4 to CO while the specific catalyst is able to oxidize CO to CO_2 at low temperature. The $Co_1Ni_1O_x$(500) catalyst under plasma-catalyst hybrid condition demonstrated the similar activity and selectivity to those of the PGM catalysts such as Pd/Al_2O_3 as shown in Figure 2-4(a). The Pd/Al_2O_3 showed complete oxidation to CO_2 thus the CO selectivity was not presented in Figure 2-4(b).

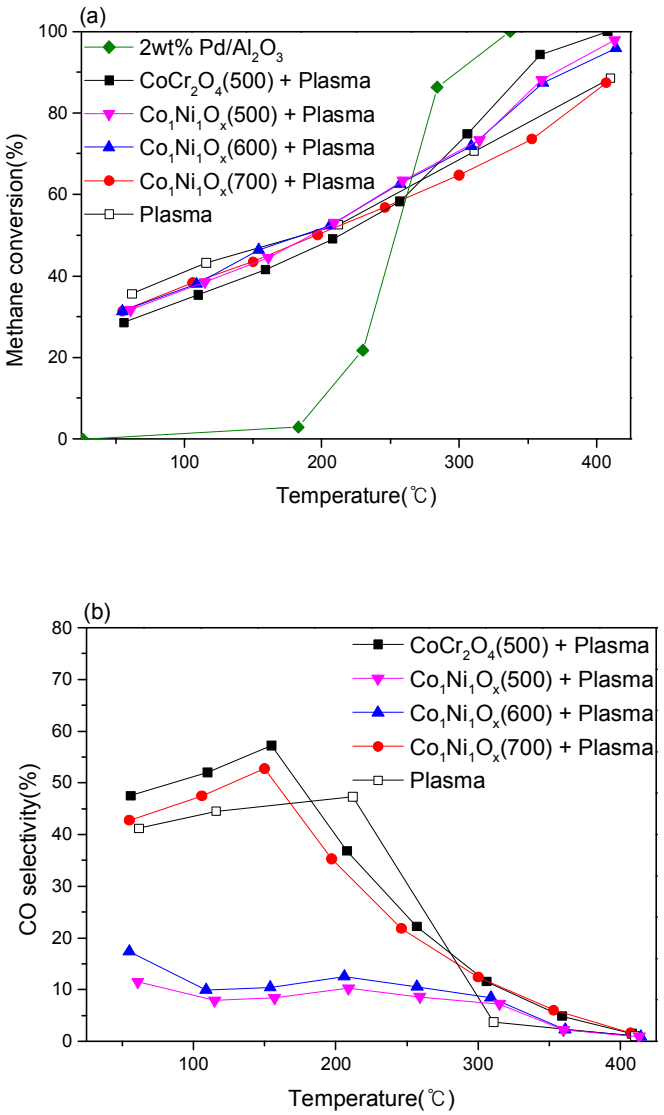

Figure 2-4. (a) Methane conversion curves of non-PGM catalysts in the plasma-catalyst hybrid system at $4kV_{p-p}$ compared with Pd/Al_2O_3, (b) CO selectivity plot over non-PGM catalysts with DBD plasma.

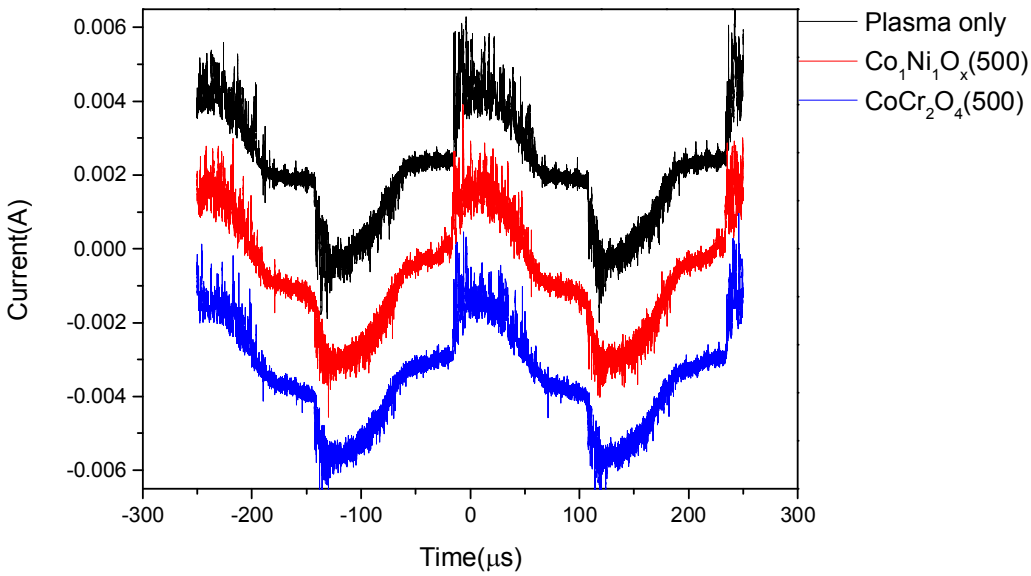

Figure 2-5. Current characteristics of the methane oxidation reaction at room temperature.

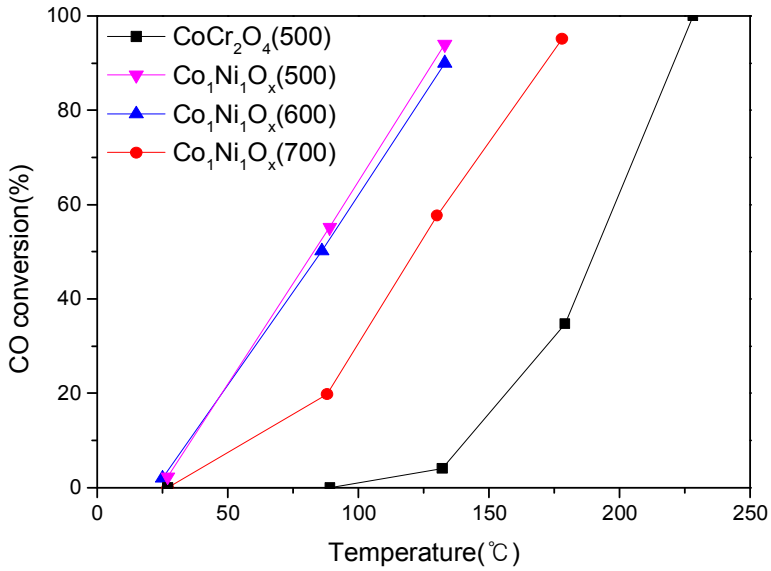

Figure 2-6. CO oxidation over $CoCr_2O_4$ and $Co_1Ni_1O_x$ catalysts (Reaction conditions: 1000ppm CO, 1% O_2, balanced in He without DBD plasma).

Chapter 3. Plasma-catalyst hybrid system using Ag/SiO_2 for oxidative coupling of methane (OCM) and subsequent regeneration at low temperature

3.1. Introduction

Methane is the major component of natural gas, which is one of the abundant fossil fuels on earth [2]. However, the utilization of methane has been limited to the route of synthesis gases to produce liquid hydrocarbons and other chemical products, which is regarded as indirect methods [4, 5]. Such indirect process has weaknesses such as high operating cost and low thermodynamic efficiency. Hence, if methane is directly utilized as alternative feedstock to petroleum, it will be highly desirable from the economic point of view. Therefore, many efforts have been made to directly convert methane into more useful products like olefins or aromatics by using various catalysts for decades [6, 7, 62-64]. Among them, direct synthesis of C_2 and C_3 hydrocarbons which are suitable for chemical feedstocks has been extensively investigated [65-67]. There are two ways to produce these hydrocarbons directly from methane with one step. One is oxidative coupling of methane (OCM) and the other is non-oxidative coupling of methane (non-OCM). Non-OCM uses only methane as reactant gas and thus the coking problem occurs seriously. On the other hand, OCM utilizes oxygen as well as methane so that it can mitigate the deactivation of catalyst arising from coking. Hence, many OCM catalysts such as Li/MgO, $Mn\text{-}Na_2WO_4/SiO_2$, and Ag catalysts have been commonly studied so far [68-71]. However, high temperature above at least 700 °C is required for these catalysts to demonstrate significant activity because methane is hardly activated due to its stable C-H bond [72-75]. In other words, it is a

difficult target to achieve only with catalyst from the practical point of view because the reaction requires high temperature which causes deactivation of the catalyst [76]. The performance of past catalysts and their activation temperature are summarized in Figure 3-1 [77, 78]. An alternative way to activate methane at lower temperature would be to use plasma [28, 79]. There are various plasma sources such as dielectric barrier discharge (DBD), corona, microwave, arc, spark, and radio frequency [16, 17], which can be divided into thermal plasma and non-thermal plasma [80, 81]. In case of thermal plasma condition, the gas temperature increases significantly to above 1000 °C since electron and bulk gas are in thermal equilibrium state [19]. Thus, such plasma is not desirable for catalytic reaction because the catalyst deactivation such as sintering can occur more severely under the reaction condition. On the other hand, the non-thermal plasma condition provides non-equilibrium condition in which temperatures of bulk gas and electron are different [82]. High-energy electrons (1–20 eV) which can initiate the formation of various reactive radicals are produced [21]. Since electron mass is very light, non-thermal plasma causes the gas temperature to increase by only a few degrees [20]. Therefore, partially ionized gas can be created in a simple reactor configuration with relatively inexpensive power source, while reaction condition would be maintained almost isothermally. Among various non-thermal plasma sources, dielectric barrier discharge (DBD) plasma has been commonly utilized by the researchers so far since it is easier to set up than other non-thermal plasma sources [61, 83-86]. Therefore, DBD plasma was used in this work as a plasma source.

In this chapter, OCM has been carried out to produce C_2 or C_3 hydrocarbons directly from methane using plasma-catalyst hybrid system with various catalysts.

Since catalyst only reaction required high temperature above 700 °C, dielectric barrier discharge (DBD) plasma, one of non-thermal plasma, was applied to lower the reaction temperature. We aimed at finding the optimum OCM catalyst to have the highest C_{2+} hydrocarbon yield at low temperature (< 400 °C) in the plasma-catalyst hybrid system, which was found to be Ag/SiO_2. In addition, the time-on-stream (TOS) activity of Ag/SiO_2 under the plasma-catalyst hybrid system was investigated. The plasma regeneration and the thermal regeneration in oxygen-rich condition were introduced to the deactivated catalyst in order to provide the appropriate regeneration strategy in the OCM reaction in plasma-catalyst hybrid system.

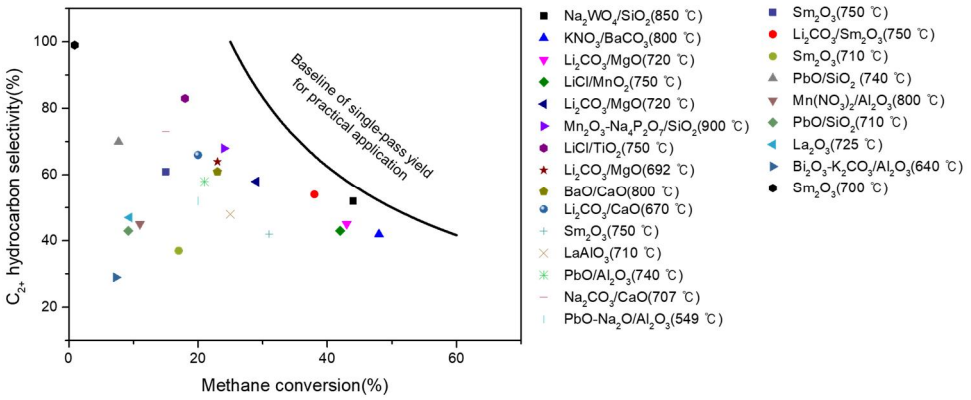

Figure 3-1. OCM performance of past catalysts and their activation temperature.

3.2. Experimental

3.2.1. Reaction system

A schematic view of plasma-catalyst hybrid system is presented in Figure 3-2. It consisted of a 1000:1 high voltage probe (Tektronics P6015A), a current probe (Pearson electronics 6585), and a capacitor (2000 pF) for measuring voltage (V), current (A), and transferred electric charge (Q), respectively. All output signals were transmitted to a 100 MHz digital oscilloscope (Tektronics DPO 2014) which was utilized to calculate discharge power by the V-Q Lissajous figure method. The system is described well in the previous paper [50].

The catalysts in bead form (30–40 mesh) were located on the quartz wool in the middle of reactor inside the plasma discharge zone. The height of catalyst bed varied from 5.0 mm to 15.0 mm because of the difference in the density of catalyst where weight of the catalyst was fixed to 0.5 g except for the case of $BaTiO_3$. In order to fill the discharge gap where the plasma was generated, the weight of $BaTiO_3$ which had high density increased to 1.0 g. The catalyst bed temperature was measured and recorded using K type thermocouple which was protected by another quartz tube just below the quartz wool in the reactor. Another thermocouple in the furnace was used to control the setting temperature.

Configuration of the plasma-catalyst hybrid reactor is shown in Figure 3-3. The DBD reactor was made of α-Al_2O_3 tube with an inner diameter of 12.0 mm, a thickness of 2.0 mm and a length of 300.0 mm. The quartz wool was located at the middle of reactor and its thickness was about 5.0 mm. In this reactor, catalyst zone and plasma zone were overlapped at the same position. Electrical discharge source of the reactor was DBD. The reactor consisted of a stainless steel rod of which thickness was 4.0 mm. The rod was located at the center of α-Al_2O_3 tube reactor.

The outer surface of the reactor was surrounded by stainless steel plate with a length of 20.0 mm and a thickness of 0.2 mm. Therefore, the length of discharge zone was 20.0 mm, and the discharge gap was 4.0 mm, resulting in a reaction volume of about 2.0 cm^3 in plasma only condition. However, in plasma-catalyst hybrid reaction, this reaction volume varied depending on the packing material since plasma could not be generated at the space occupied by the packing material. To create the discharge, an AC high voltage was generated with a maximum of 7.5 kV_{P-P} by an arbitrary function generator (GW INSTEK AFG-2012) and amplified by a high voltage amplifier (TREK 20/20C-HS) with a maximum peak voltage of 20 kV_{P-P} and a variable frequency of up to 20 kHz. All experiments were carried out under the identical conditions of sinusoidal waveform with the driving frequency of 4 kHz.

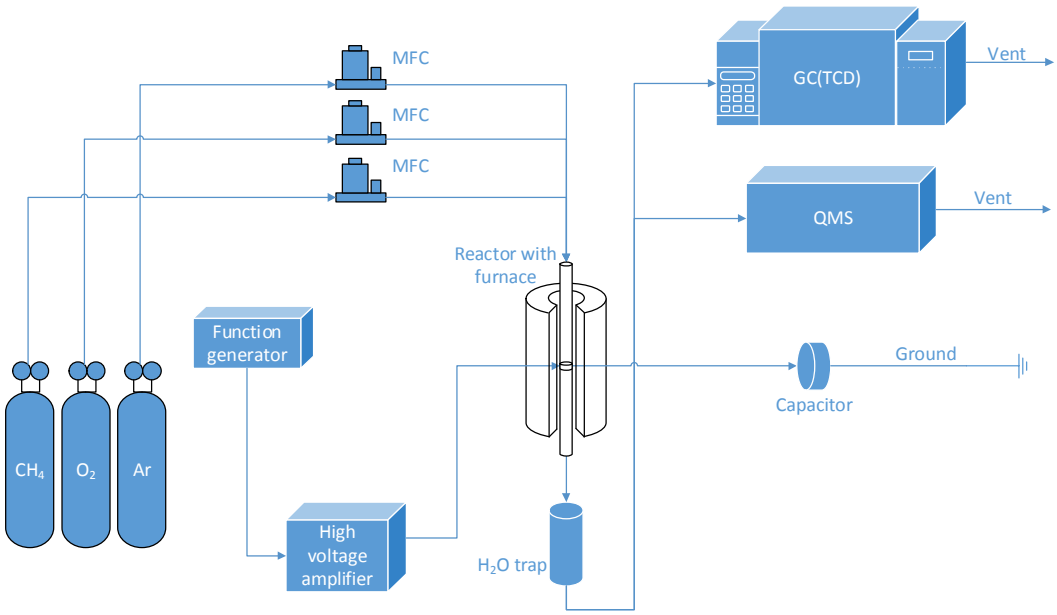

Figure 3-2. Schematic view of plasma-catalyst hybrid system.

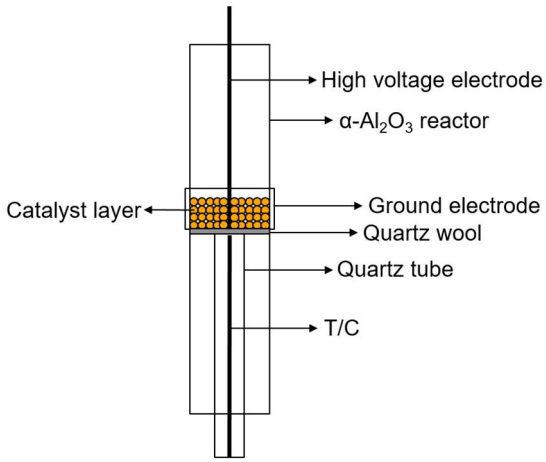

Figure 3-3. Shape of plasma-catalyst hybrid reactor.

3.2.2. Preparation of catalysts

Commercial supports such as $BaTiO_3$ (Sigma Aldrich), TiO_2 (Millennium Inorganic Chemicals), γ-Al_2O_3 (Sasol), fumed SiO_2 (Sigma Aldrich), and glass bead (Sigma Aldrich, 30–40 mesh) were utilized to investigate the effect of support under DBD plasma condition. Then, various metals were loaded on SiO_2 by using wet impregnation method. $Pd(NO_3)_2 \cdot 2H_2O$ (Sigma Aldrich), $Pt(NH_3)_4(NO_3)_2$ (Alfa Aesar), $AgNO_3$ (Sigma Aldrich), $Co(NO_3)_2 \cdot 6H_2O$ (Sigma Aldrich), $Ni(NO_3)_2 \cdot 6H_2O$ (Alfa Aesar), $Cu(NO_3)_2 \cdot 3H_2O$ (Sigma Aldrich), $Pb(NO_3)_2$ (Sigma Aldrich), $RuCl_3 \cdot xH_2O$ (Sigma Aldrich), $RhCl_3 \cdot xH_2O$ (Sigma Aldrich), $IrCl_4 \cdot xH_2O$ (Sigma Aldrich), and NaCl (SAMCHUN PURE CHEMICAL) were used as metal precursor. The loading amount of each metal was fixed to 2 wt% of the catalyst. The catalysts were dried and subsequently calcined in static air at 500 °C for 2 h. Then, the catalysts were sieved to the particle size of 30–40 mesh. Solid-state phases were identified by using X-Ray Diffraction (RIGAKU SMARTLAB) operated at 40 kV and 50 mA. Surface area of the catalysts was also obtained by using the N_2 adsorption/desorption method in an ASAP 2010 instrument (Micromeritics Co.).

3.2.3. Activity measurement

All of the reaction results including catalyst only reaction, plasma only reaction, and plasma-catalyst hybrid reaction were measured at atmospheric pressure in the same α-Al_2O_3 reactor. The reactants were 24% CH_4, 6% O_2, balanced in Ar. The total gas flow rate was 100 ml/min. Each gas was controlled by using mass flow controllers (SIERRA). Effluent gases passing through the discharge region went through the water trap and were analyzed by a gas chromatography (AGILENT GC

6890N) equipped with a thermal conductivity detector (TCD) and CP-7429 capillary column. The column was composed of two parallel columns (CP-Molsieve 5Å and PoraBOND Q) which allowed us to detect H_2, O_2, CO, CH_4, CO_2, C_2H_2, C_2H_4, C_2H_6, C_3H_6, and C_3H_8. Among the reaction products, C_{2+} hydrocarbon includes C_2H_2, C_2H_4, C_2H_6, C_3H_6, and C_3H_8 in this experiment. Methane consumption except the amount used for hydrocarbon production was regarded as being consumed for coke formation. The activity of the hybrid system was measured at 20 min after the OCM reaction started except the case of time-on-stream reaction. Methane conversion and C_{2+} hydrocarbon yield were obtained while temperature was varied from room temperature to about 700 ℃ in the presence and in the absence of catalyst. Conversion of methane, and selectivity and yield of CO, CO_2, and hydrocarbons are obtained in the following:

$$\text{Conversion}(CH_4) = \frac{mol(consumed\ CH_4)}{mol(introduced\ CH_4)} \times 100[\%] \quad (6)$$

$$\text{Selectivity}(\text{CO}) = \frac{mol(formed\ CO)}{mol(converted\ CH_4)} \times 100[\%] \quad (7)$$

$$\text{Selectivity}(CO_2) = \frac{mol(formed\ CO_2)}{mol(converted\ CH_4)} \times 100[\%] \quad (8)$$

$$\text{Selectivity}(\text{HC}) = \frac{mol(formed\ HC) \times CN(formed\ HC)}{mol(converted\ CH_4)} \times 100[\%] \quad (9)$$

$$\text{Yield}(\text{HC}) = \frac{Conversion(CH_4) \times Selectivity(HC)}{100}[\%] \quad (10)$$

Where CN and HC stands for carbon number and C_{2+} hydrocarbon, respectively.

In addition to the gas chromatography, quadrupole mass spectrometer (QMS, Pfeiffer Vacuum, Prisma^{TM} QMS 200) was utilized to detect the product in real time. Especially, QMS was applied for the O_2 temperature-programmed desorption (O_2 TPD) and the detection of coke oxidation to CO and CO_2. Before O_2 TPD,

oxygen plasma treatment was applied at the same condition as OCM reaction except the gas ratio (30% O_2, balanced in Ar) for 30 min.

3.2.4. Regeneration procedure

Long term activity test was conducted at 385 ℃ for 180 min in plasma-catalyst hybrid system. After the reaction for 180 min, two regeneration processes were carried out: plasma regeneration and thermal regeneration. The plasma regeneration proceeded in the condition of 30% O_2 balanced in Ar at 378 ℃ for 30 min in order not to alter the total flow rate and the proportion of Ar, discharge gas. Thermal regeneration was applied at 600 ℃ for 30 min after ramping from room temperature to 600 ℃ at 5 ℃/min.

3.3. Results and discussion

3.3.1. Oxidative coupling of methane under plasma only condition

The first set of experiment was conducted under plasma only condition in order to establish a reference for plasma-catalyst hybrid reaction. In case of plasma only reaction, methane conversion and C_{2+} hydrocarbon selectivity were measured from room temperature to 397 °C at 7.5 kV_{P-P}. The results are summarized in Figure 3-4 and Table 3-1. At about 400 °C, plasma only reaction reached the methane conversion of 21.3% and the C_{2+} hydrocarbon yield of 4.7%. Depending on the temperature, DBD showed the plasma power from 5.0 W to 8.6 W. As described in Figure 3-4, the growth in C_{2+} hydrocarbon yield with increasing temperature could be ascribed to the fact that more reactive species like electrons were generated because of the higher plasma power. Methane conversion and C_{2+} hydrocarbon selectivity in DBD increased as the reaction temperature went up as described in Table 3-1. Figure 3-5 demonstrates that the majority of the product was CO (60.4%) and most abundant hydrocarbon product was C_2H_6 (17.0%), which corresponded well with previous reports about the coupling of methane under plasma condition [87-89]. Such product distribution was attributed to the fact that the OCM reaction at relatively low plasma power started commonly from the dissociation of methane molecules to produce methyl radicals which were readily combined to form C_2H_6. As the temperature went up, both methane conversion and C_{2+} hydrocarbon selectivity increased as shown in Table 3-1 at the same input voltage and frequency under DBD plasma condition. In Figure 3-6, Lissajous plots of DBD plasma are demonstrated in addition to the plasma power calculated from the plots at each temperature. The plasma discharge power can be calculated by the multiplication of capacitor value, plasma frequency, and area of Lissajous figure [50]. The lines

(A-B) and (C-D) in Figure 3-6 indicate the discharge transitions, and their slope is equal to dielectric capacitance. Line (B-C) and (D-A) are capacitive transitions of which slope are equal to total capacitance [30]. According to Figure 3-6, it was identified that the dielectric capacitance increased as the reaction temperature went up, resulting in the increased plasma power.

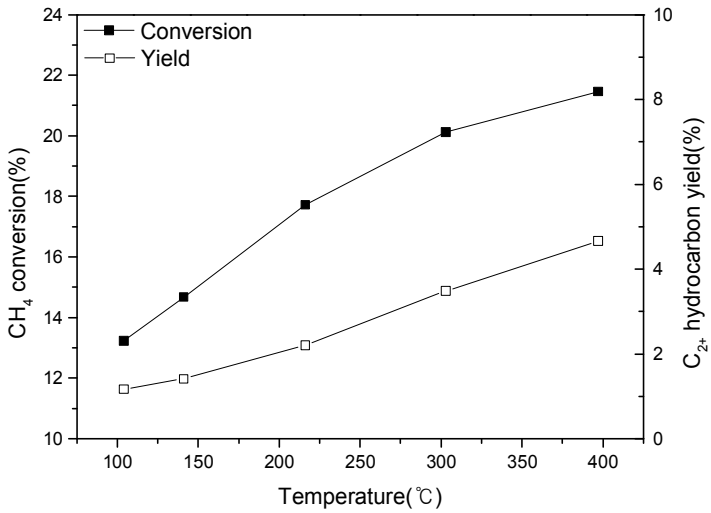

Figure 3-4. Methane conversion and C_{2+} hydrocarbons yield of plasma only reaction.

Table 3-1. Methane conversion, oxygen conversion, and C_{2+} hydrocarbon selectivity under plasma only condition.

Plasma only			
Temp.	Conversion (%)		C_{2+} hydrocarbon selectivity
(ºC)	CH_4	O_2	(%)
104	13.2	57.3	8.9
141	14.7	62.0	9.6
216	17.7	71.0	12.4
303	20.1	75.0	17.3
397	21.5	81.4	21.7

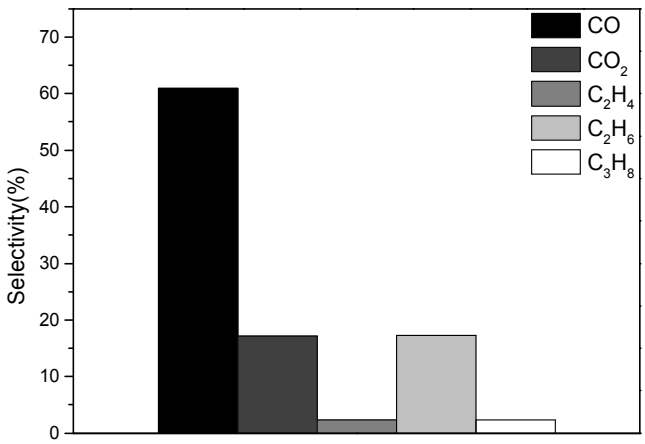

Figure 3-5. Selectivity of the reaction products in the condition of DBD plasma only at about 400 ºC.

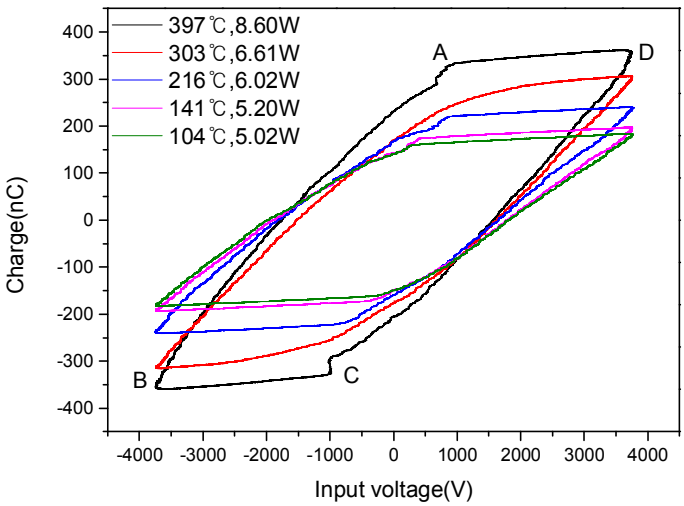

Figure 3-6. Plasma power with increasing temperature measured by Lissajous method in the condition of DBD plasma only.

3.3.2. Oxidative coupling of methane with various supports under plasma condition at low temperature

OCM reaction over the conventional catalysts under the catalytic system requires high reaction temperature as mentioned above. Thus, a new approach of low reaction temperature using plasma-catalyst hybrid system was devised in this research. At first, various supports such as γ-Al_2O_3, TiO_2, and $BaTiO_3$ as well as SiO_2 were applied under DBD plasma condition to investigate which support was appropriate for OCM under the plasma condition at low temperature (< 400 °C). As displayed in Figure 3-7, OCM under DBD plasma condition with various supports was carried out from ambient temperature to about 400 °C. Among the support materials, SiO_2 showed higher C_{2+} hydrocarbon yield than plasma only reaction in a plasma-catalyst hybrid system. According to Table 3-2 showing dielectric constant and surface area of the supports, hydrocarbon yield of the supports under plasma condition was inversely proportional to the dielectric constant of the supports. There are some controversial opinions about the relationship between dielectric constant and plasma-catalytic performance [57, 90-92]. However, according to Wang et al. [93], the net electric field decreases due to the accumulation of electrons on the solid surface, especially for the supports with large dielectric constant, resulting in the decreased activity. Besides the dielectric constant, large surface area of the support could have a beneficial effect on the charge accumulation over the surface, which can lead to the formation of enhanced discharge. For this reason, the hydrocarbon yield might be proportional to the surface area of the supports. Hence, glass bead, which has same dielectric constant with SiO_2 but much smaller surface area, was tested to examine the effect of surface area on the activity compared with SiO_2. As shown in Figure 3-7, the

activity result confirmed that glass bead showed similar synergistic effect to SiO_2. Therefore, dielectric constant seemed to play a crucial role in the OCM performance when using various support materials with plasma.

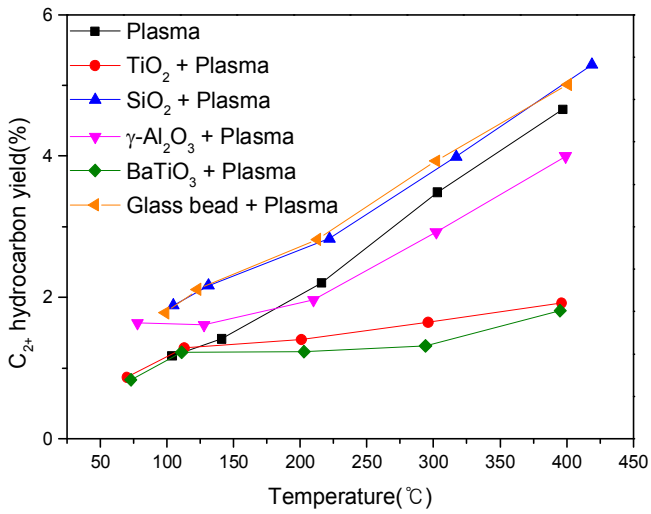

Figure 3-7. C_{2+} hydrocarbon yield under dielectric barrier discharge plasma condition using various supports.

Table 3-2. Specific surface area and dielectric constant of the supports.

Support	Specific surface area(m^2/g)	Dielectric constant of support(ε) [94-97]
$BaTiO_3$	2	1200–10000
TiO_2	84	80
γ-Al_2O_3	257	9
SiO_2	367	3.9
Glass bead	<1	3.9

3.3.3. Ag/SiO_2 catalyst under plasma-catalyst hybrid system

3.3.3.1.Oxidative coupling of methane over various SiO_2-supported catalysts

It was proposed that the performance of catalysts was proportional to that of supports in plasma-catalyst hybrid system [93]. Because SiO_2 showed the best performance among the supports under DBD plasma condition, various metals were loaded on SiO_2. The amount of metal was fixed to 2 wt%. XRD patterns of the catalysts (not shown) demonstrated that only the peaks assigned to the amorphous SiO_2 existed without any metal-related peaks, indicating that the metal species were highly dispersed over SiO_2 surface. Among various metals (Pb, Pt, Pd, Ni, Ag, Ru, Na, Rh, Ir, Cu, and Co), Ag revealed the highest hydrocarbon yield at 385 °C as shown in Figure 3-8. The Ag on SiO_2 catalyst showed the hydrocarbon yield of 9.7% at the reaction temperature of 385 °C. In order to evaluate the synergistic effect of the reaction, the synergistic effect factor was introduced. The synergistic effect factor was defined as the yield of C_{2+} hydrocarbon in plasma-catalyst hybrid reaction, divided by the sum of C_{2+} hydrocarbon yield in plasma only and catalyst only reaction. The synergistic effect factor was calculated by using Eq. (11):

$$\text{Synergistic effect factor} = \frac{Y_{HC(P-C)}}{Y_{HC(P)} + Y_{HC(C)}} \times 100\ [\%] \qquad (11)$$

Where $Y_{HC(P-C)}$, $Y_{HC(P)}$, and $Y_{HC(C)}$ indicates the C_{2+} hydrocarbon yield under plasma-catalyst hybrid system, the C_{2+} hydrocarbon yield with plasma only, and the C_{2+} hydrocarbon yield with catalyst only, respectively.

Surface area and synergistic effect factor of the catalysts are presented in Table 3-3. All values of synergistic effect factor in Table 3-3 were calculated based on the activity result at close to 400 °C. In addition, the catalyst only reaction did not

present any C_{2+} hydrocarbon yield at reaction temperature below 400 °C and thus $Y_{HC(P)} + Y_{HC(C)}$ was equal to $Y_{HC(P)}$. The synergistic effect factor shows the correlation among plasma-catalyst hybrid reaction, plasma only reaction, and catalyst only reaction. If the yield of hybrid reaction is equal to the sum of plasma only and catalyst only reaction yields, the synergistic effect will be 100%. Therefore, the value of synergistic effect factor above 100% indicates that a synergistic effect existed on OCM under plasma-catalyst hybrid system. Table 3-3 indicates that Ag/SiO_2 demonstrates high value of synergistic effect factor (209%) in the plasma-catalyst hybrid reaction at about 400 °C. In addition, the maximum plasma power in this study was about 8.4 W (5.1 kJ/L, Figure 3-9), which was much lower than that of previous works (17.7 kJ/L–45.0 kJ/L) [79, 98-100]. Therefore, it can be mentioned that the synergistic effect between plasma and Ag/SiO_2 is remarkable. Since the addition of Ag/SiO_2 catalyst did not lead to change of plasma power in spite of the increased total capacitance, it can be claimed that the synergistic effect did not arise from plasma configuration but from interaction between plasma and catalyst. According to Bao et al. [101], Ag catalysts were verified to be active for OCM when it was applied under oxygen-limited condition at atmospheric pressure, which is consistent with our result.

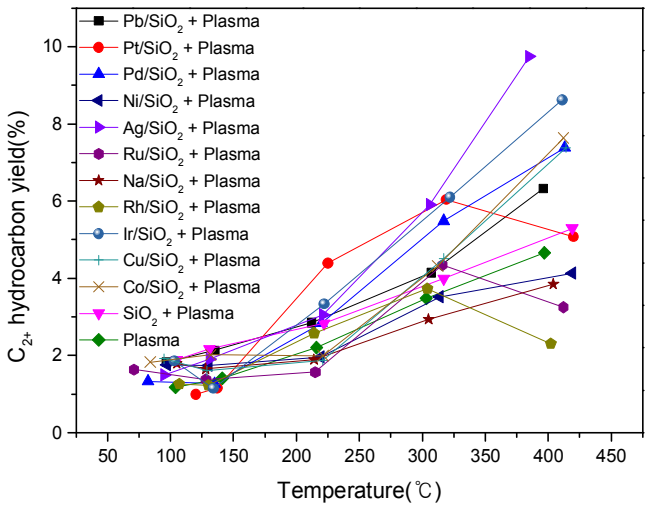

Figure 3-8. Oxidative coupling of methane performance under plasma condition using various metals on SiO_2.

Table 3-3. Specific surface area and synergistic effect factor of the catalysts

Catalyst	Specific surface area (m^2/g)	Synergistic effect factor
Pb/SiO_2	323	136%
Pt/SiO_2	341	109%
Pd/SiO_2	331	158%
Ni/SiO_2	324	89%
Ag/SiO_2	308	209%
Ru/SiO_2	350	70%
Na/SiO_2	351	83%
Rh/SiO_2	312	48%
Ir/SiO_2	345	185%
Cu/SiO_2	365	158%
Co/SiO_2	322	164%

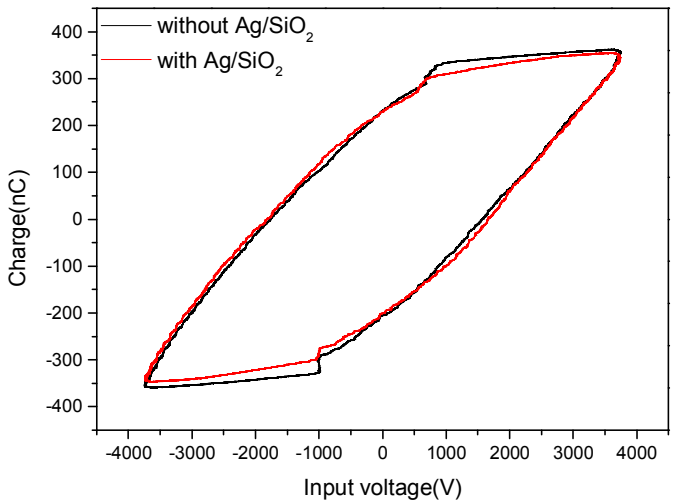

Figure 3-9. Lissajous plot of DBD plasma with and without Ag/SiO_2 at about 400 ºC, 7.5kV_{P-P}.

3.3.3.2.Role of oxygen in oxidative coupling of methane under plasma-catalyst hybrid system

Methane conversion, C_{2+} hydrocarbon yield, and carbon product selectivity under the reaction condition of OCM at about 400 °C are displayed in Figure 3-10. As shown in Figure 3-10, 2 wt% Ag/SiO_2 demonstrated synergistic effect in the presence of oxygen (from 4.7% to 9.7% with regard to C_{2+} hydrocarbon yield). Furthermore, OCM reaction in plasma-catalyst hybrid system with Ag/SiO_2 showed carbon balance above 95% in 20 min of reaction, which meant that little amount of coke was formed. In addition, compared with OCM reaction under plasma only condition, selectivity of olefin products such as C_2H_4 and C_3H_6 increased in the plasma-catalyst hybrid system, representing that methane was dissociated more abundantly over Ag/SiO_2 in the presence of oxygen. This led to the result that Ag/SiO_2 could alter the reaction pathway of OCM. According to Rocha et al. [102], different oxygen species could be created on and in the Ag catalyst. Among the oxygen species, O_γ were assigned to strongly bound, intercalated oxygen which diffused via interstitialcy diffusion into the uppermost layers of the reconstructed Ag surface, where it might react with gaseous reactants [103]. Such subsurface oxygen (O_γ) was suggested to react with methane to give the dehydrogenation of methane to methyl radical [104]. Ag metal played a role as the active catalyst for oxi-dehydrogenation while O_γ worked for pure dehydrogenation. In the plasma condition, O_γ might be generated at relatively low temperature since the specific input energy by plasma (273.7 kJ/mol at 1 atm, 385 °C, assuming ideal gas) was sufficiently higher than the activation energy of oxygen diffusion in Ag (140.0 kJ/mol) which was regarded as the rate determining step of the reaction [105]. Hence, the generation of O_γ led to H abstraction from

methane molecule, which resulted in the coupling of methane. In order to identify the existence of O_γ, O_2 temperature-programmed desorption (O_2 TPD) was conducted by using QMS after the oxygen plasma treatment for 30 min. As shown in Figure 3-11, the oxygen peak originated from O_γ after the oxygen plasma treatment was observed at about 800 °C, consistent with the result of Nagy et al. [104]. Note that 0.5 g of 2 wt% Ag/SiO_2 (i.e. Ag 0.01 g) was applied in this study whereas 1.0 g of Ag was used in the reference. Therefore, the peak size was far smaller than the reference one. Nevertheless, it can be said that O_γ which is active for the dehydrogenation of methane was generated by the plasma treatment at much lower temperature (380 °C) compared to catalyst only reaction that requires high temperature above 600 °C. This is in good agreement with the conclusion of Xu et al. [106] who mentioned that subsurface oxygen increased the reactivity of the Ag surface and enhanced the kinetics of H_2 dissociation substantially based on density functional theory calculations. Furthermore, the selectivity of C_2H_4 and C_3H_6 that were formed by H abstraction from C_2H_6 and C_3H_8, respectively, increased in the presence of oxygen. This confirmed that the role of oxygen (O_γ) was important for the dehydrogenation of saturated hydrocarbons as well as methane, which resulted in the production of unsaturated hydrocarbons.

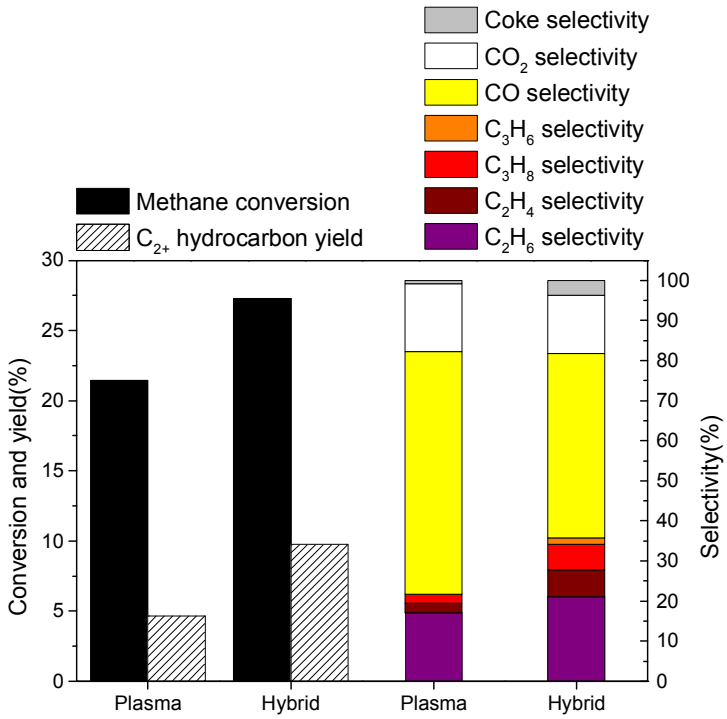

Figure 3-10. Methane conversion, hydrocarbon yield and product selectivity in the condition of oxidative coupling of methane at about 400 ℃ after reaction for 20 min; Hybrid=2 wt% Ag/SiO_2 + Plasma.

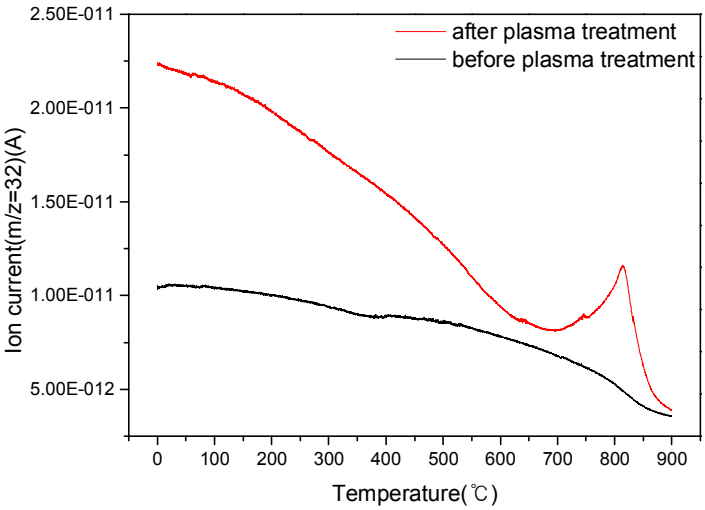

Figure 3-11. Oxygen temperature-programmed desorption (O_2 TPD) of Ag/SiO_2 pretreated in oxygen plasma from room temperature to 900 °C with the ramping rate of 2 °C/min.

3.3.4. Long term activity of plasma-catalyst hybrid system for oxidative coupling of methane

Long term activity of the catalyst was explored in order to utilize in practical application. Figure 3-12 shows the methane conversion, C_{2+} hydrocarbon selectivity, and C_{2+} hydrocarbon yield of Ag/SiO_2 in the plasma-catalyst hybrid system with time-on-stream (TOS). As shown in Figure 3-12, both methane conversion and C_{2+} hydrocarbon selectivity decreased as the reaction proceeded. At first, fresh Ag/SiO_2 revealed 9.7% of C_{2+} hydrocarbon yield. However, after 180-min TOS in the plasma-catalyst hybrid system, the yield dropped to 5.9%. At the same time, the color of the catalyst turned to dark brown in addition to the deposition of black carbon on the surface of high voltage electrode and reactor wall. Such carbon deposition is expected to have the detrimental effect on both catalyst and plasma.

Therefore, the regeneration process was applied in order to recover the reactivity of plasma-catalyst hybrid system by eliminating the carbon deposition. Two regeneration methods were designed: plasma regeneration and thermal regeneration. The plasma regeneration was carried out for 30 min at 378 °C. The specific input energy in the plasma regeneration was calculated to 290.1 kJ/mol (Figure 3-13, at 1 atm, 378 °C, assuming ideal gas). The evolution of CO and CO_2 during plasma regeneration on aged Ag/SiO_2 measured by QMS is demonstrated in Figure 3-14(a). As shown in Figure 3-14(a), oxidation of the carbon deposition to CO and CO_2 (mostly to CO_2) started immediately as plasma was turned on. This was attributed to the formation of reactive oxygen species, which could easily interact with the carbon deposition to produce CO and CO_2. To ensure the effect of oxygen plasma regeneration, thermal regeneration was applied to the post-reaction catalyst at same

gas ratio with the plasma regeneration. Figure 3-14(b) demonstrates the evolution of CO and CO_2 during thermal regeneration on aged Ag/SiO_2 observed by QMS. In case of thermal regeneration, most of the coke did not react until temperature reached about 500 °C while the plasma regeneration started instantly at 378 °C. This can be attributed to the deficiency of reactive bulk oxygen species that promotes the oxidation of carbon deposition in the case of thermal regeneration. When the temperature reached about 500 °C, the MS signals of CO and CO_2 began to increase. The thermal regeneration reaction was carried out until MS signals of CO and CO_2 became stabilized and flattened. After each regeneration processes, OCM reaction over the regenerated catalysts proceeded in the plasma-catalyst hybrid system. The OCM reaction result of two regenerated catalysts compared with fresh one in the plasma-catalyst hybrid system is displayed in Figure 3-15. Plasma regenerated Ag/SiO_2 catalyst showed completely recovered activity, while the thermally regenerated one partially did (7.3% of C_{2+} hydrocarbon yield). In addition, as OCM reaction went on over the latter sample, the deactivation got much worse. In order to identify the influence of plasma regeneration and thermal regeneration on catalyst, X-Ray Diffraction (XRD) was taken. As displayed in Figure 3-16, XRD pattern of the fresh Ag/SiO_2 shows that only the peaks assigned to the amorphous SiO_2 existed without any metal-related peaks, indicating that the Ag was highly dispersed over the SiO_2 surface. Crystalline phase of Ag is hardly seen after plasma regeneration although the catalyst exhibited highly crystalline Ag (JCPDS 65-2871) phase after the thermal regeneration. Therefore, it can be claimed that sintering of Ag took place significantly during the thermal regeneration. Since the catalyst was initially calcined at 500 °C, thermal regeneration above 500 °C can give rise to Ag sintering, which resulted in the deactivation of the catalyst.

Furthermore, aged catalyst after the plasma regeneration even showed the better C_{2+} hydrocarbon yield (10.5%) than fresh catalyst at the beginning of the reaction. This can be explained by the fact that additional O_γ formed during plasma regeneration improved the dehydrogenation of methane without sintering of Ag.

Besides, additional regeneration by plasma at about 378 °C was conducted on the thermally regenerated Ag/SiO_2 to verify whether the imperfect thermal regeneration was caused by sintering of the catalyst. CO and CO_2 peaks were detected again by QMS during plasma regeneration, which implies that residual carbon deposition still existed after thermal regeneration (Figure 3-17). Furthermore, it was confirmed that after the additional regeneration by plasma, the reactivity of plasma-catalyst hybrid system was restored to 9.0%. However, the reactivity was not fully recovered even after the additional regeneration by plasma because of Ag sintering. From the results, it was confirmed that both sintering of the catalyst and residual carbon deposition on the catalyst contributed to the partial recovery after thermal regeneration.

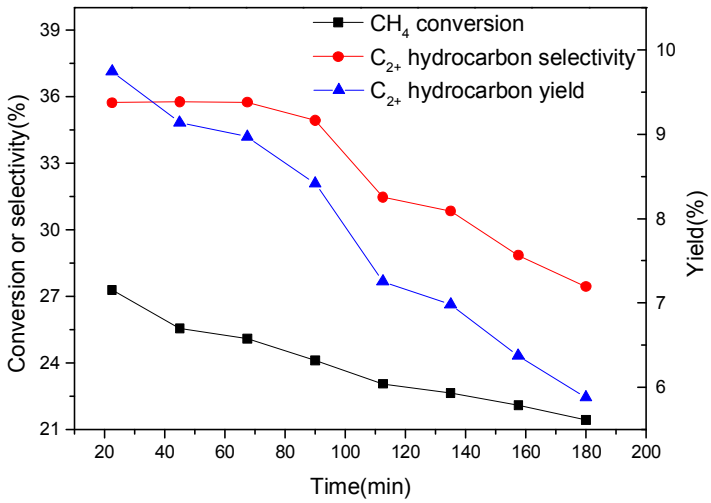

Figure 3-12. Methane conversion, C_{2+} hydrocarbon selectivity, and C_{2+} hydrocarbon yield of plasma-catalyst hybrid system with time-on-stream.

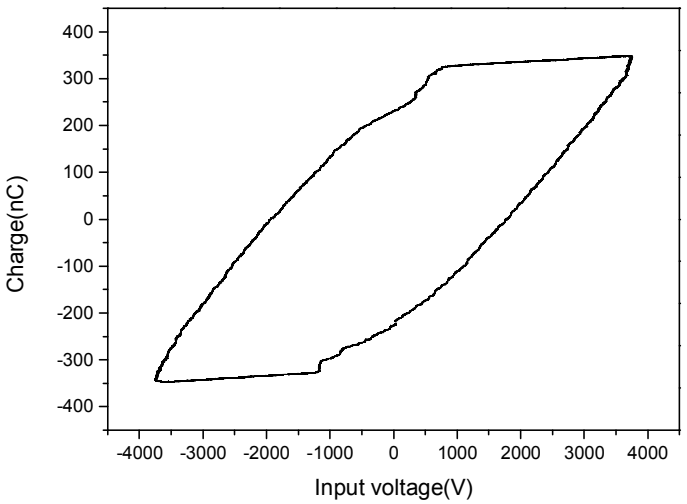

Figure 3-13. Lissajous plot of plasma regeneration for aged Ag/SiO_2 at 378 °C, $7.5kV_{P-P}$, 30% O_2, balanced in Ar.

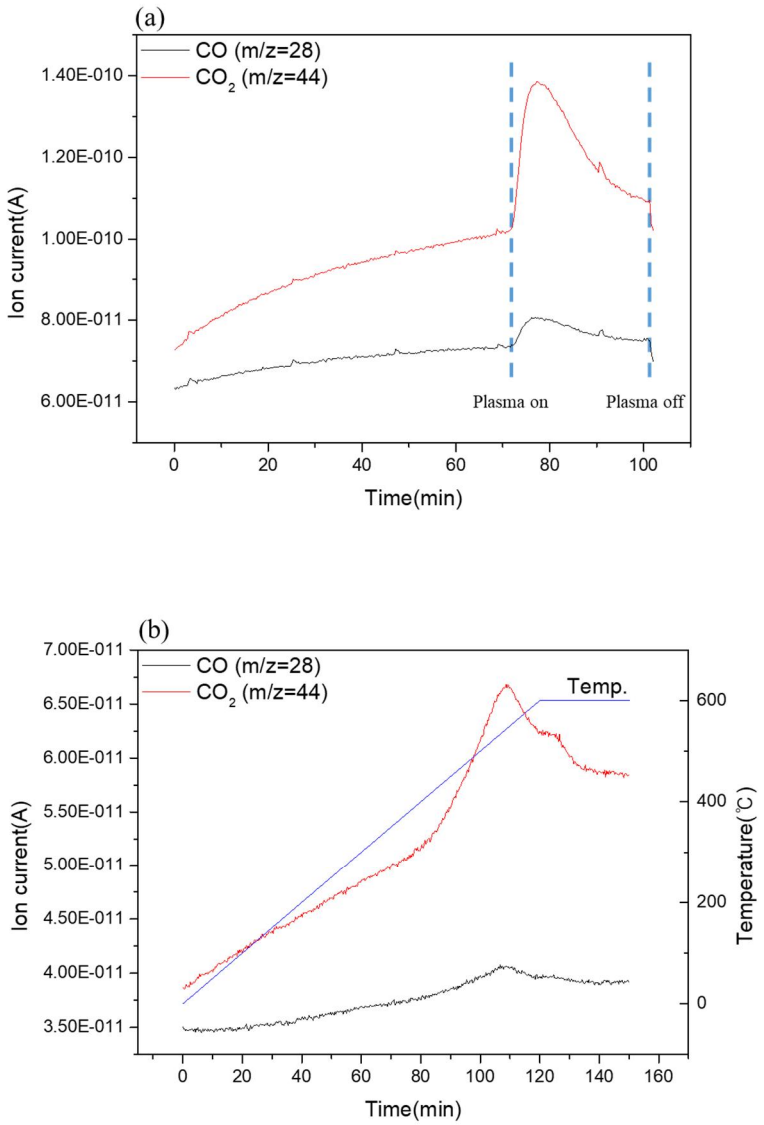

Figure 3-14. The evolution of CO and CO_2 during plasma regeneration (a) and thermal regeneration (b) measured by quadrupole mass spectrometry (QMS).

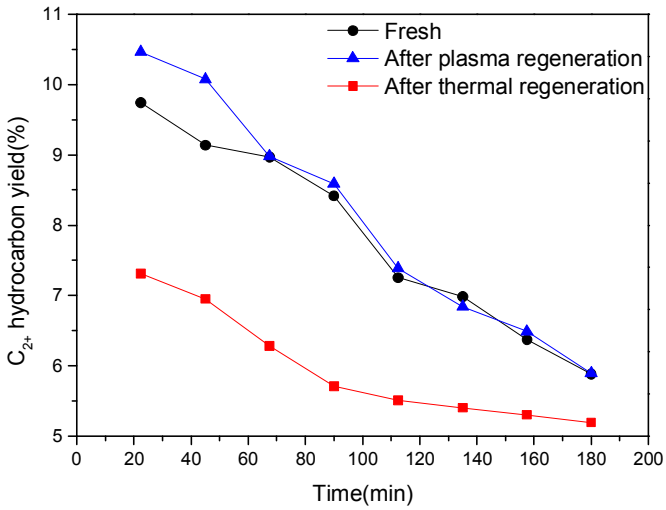

Figure 3-15. Oxidative coupling of methane (OCM) reaction results of fresh Ag/SiO_2, aged Ag/SiO_2 after thermal regeneration, and aged Ag/SiO_2 after plasma regeneration.

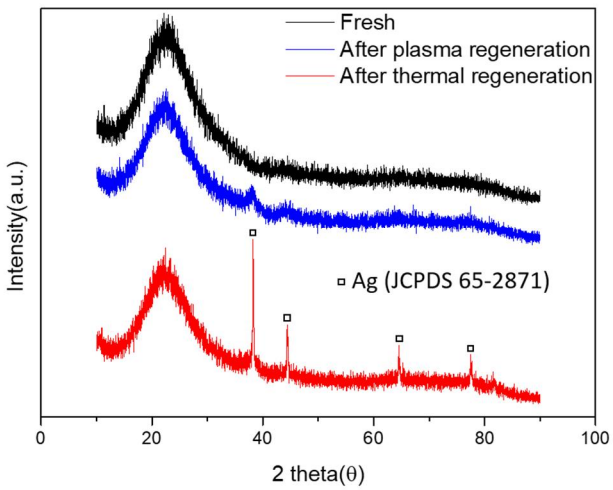

Figure 3-16. X-Ray Diffraction (XRD) patterns of fresh Ag/SiO_2, aged Ag/SiO_2 after plasma regeneration, and aged Ag/SiO_2 after thermal regeneration.

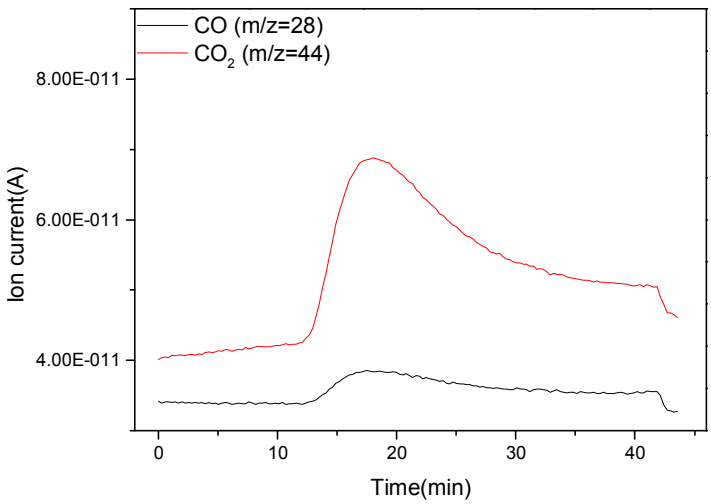

Figure 3-17. The result of additional plasma regeneration for 30 min following thermal regeneration. (O_2 30 sccm Ar 70 sccm, aged for 180 min in a plasma-catalyst hybrid system)

Chapter 4. Direct conversion of methane to methanol over metal oxide-coated glass bead in plasma-catalyst hybrid system

4.1. Introduction

Methane is a main component of natural gas, the large reserves of which is spread all over the world [107]. Therefore, methane conversion to value-added products has drawn much attention because of scientific and industrial significance. Currently, the production of methanol from natural gas should go through the formation of synthesis gas, which is considered to be inefficient. Thus, direct methanol synthesis from methane has been steadily investigated by many researchers [108-110]. However, direct methanol synthesis by catalytic reaction has limitations, since large amount of thermal energy is required to selectively activate C-H bond. Unfortunately, the applied thermal energy causes the oxidation of methane to CO or CO_2. To prevent this circumstance, batch reaction using liquid phase reactants under high pressure has been utilized [64, 111-113]. Though it could enhance the methanol selectivity, it showed still low methanol yield and it should have separation and regeneration processes.

In this chapter, the plasma was introduced to overcome the difficulties. Plasma can activate methane to produce methyl radical at lower temperature [28]. The non-thermal plasma was applied in this study since it can provide non-equilibrium condition in which temperatures of bulk gas and electron are different [82]. Among various non-thermal plasma sources, dielectric barrier discharge (DBD) plasma has been commonly utilized by the researchers so far since it is easier to set up than other non-thermal plasma sources [61, 83, 84]. Therefore, DBD plasma was used in

this work as a plasma source. It was designed that plasma acted for methane activation and catalyst played a role in enhancing methanol selectivity in the continuous packed bed reactor.

4.2. Experimental

4.2.1. Reaction system

An overall view of plasma-catalyst hybrid system is presented in Figure 4-1. It consisted of a 1000:1 high voltage probe (Tektronics P6015A), a current probe (Pearson electronics 6585), and a capacitor (2000 pF) for measuring voltage (V), current (A), and transferred electric charge (Q), respectively. All output signals were transmitted to a 100 MHz digital oscilloscope (Tektronics DPO 2014) which was utilized to calculate discharge power by the V-Q Lissajous figure method. The system is described well in the previous paper [50].

The catalysts in bead form (2.0 mm) were located on the quartz wool in the middle of reactor inside the plasma discharge zone. The height of catalyst bed exceeded 20.0 mm in order to fill the discharge gap where the plasma was generated. The catalyst bed temperature was measured and recorded using K type thermocouple which was protected by another quartz tube just below the quartz wool in the reactor.

Configuration of the plasma-catalyst hybrid reactor is shown in Figure 4-2. In this reactor, catalyst zone and plasma zone were overlapped at the same position. Electrical discharge source of the reactor was DBD. The reactor consisted of a stainless steel rod of which thickness was 4.0 mm. The outer surface of the reactor was surrounded by stainless steel plate with a length of 20.0 mm and a thickness of 0.2 mm. Therefore, the length of discharge zone was 20.0 mm, and the discharge gap was 4.0 mm, resulting in a reaction volume of about 2.0 cm^3 in plasma only condition. However, in plasma-catalyst hybrid reaction, this reaction volume decreased due to the packing materials since plasma could not be generated at the space occupied by them. To create the discharge, an AC high voltage was generated

with a maximum of 8.5 kV_{P-P} by an arbitrary function generator (GW INSTEK AFG-2012) and high voltage amplifier (TREK 20/20C-HS). All experiments were carried out under the identical conditions of sinusoidal waveform with the driving frequency of 4 kHz.

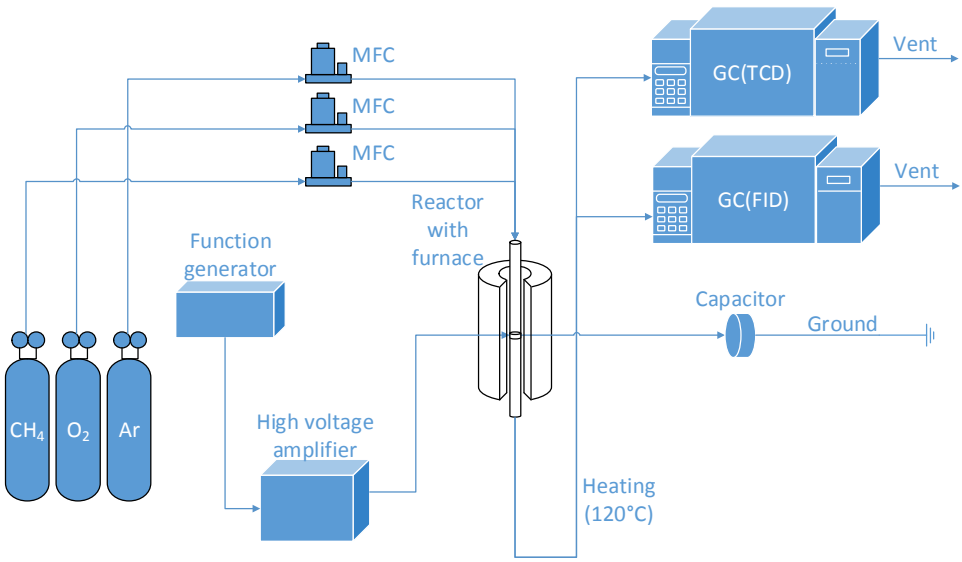

Figure 4-1. Schematic view of overall reaction system.

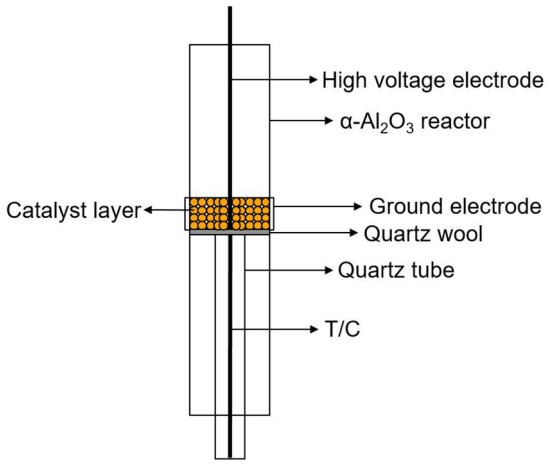

Figure 4-2. Configuration of the plasma-catalyst hybrid reactor.

4.2.2. Preparation of catalyst

Commercial borosilicate glass bead (Sigma Aldrich) was utilized as a support under DBD plasma condition. Then, various metal oxides were loaded on the spherical glass bead. The catalyst was prepared by following procedure [114]. The glass beads were etched with 5 M NaOH solution at 100 °C followed by immersing it in a suspension of metal oxide. Next, the mixture was dried at 120 °C for 1 h and washed with distilled water. The operation was repeated several times until the glass beads were no longer transparent with desired content of metal oxide. MnO (Sigma Aldrich), Mn_2O_3 (Sigma Aldrich), MnO_2 (Sigma Aldrich), Fe_2O_3 (Sigma Aldrich), NiO (Sigma Aldrich), and Co_3O_4 (Sigma Aldrich) were used as metal oxides. Specific surface area of catalysts was also obtained by using the N_2 adsorption/desorption method in an ASAP 2010 instrument (Micromeritics Co.).

4.2.3. Activity measurement

All of the reaction results including plasma only reaction and plasma-catalyst hybrid reaction were measured at atmospheric pressure in the same α-Al_2O_3 reactor. The reactants were 20% CH_4, 10% O_2, balanced in Ar. The total gas flow was maintained at 100 ml/min. Each gas was controlled by using mass flow controllers (SIERRA). Effluent gases passing through the discharge region were analyzed by a gas chromatography (AGILENT GC 6890N) equipped with a thermal conductivity detector (TCD) and a flame ionization detector (TCD). The line from the latter part of the reactor to the gas chromatography was heated up to 120 ºC, so all products were vaporized. The columns inside the GC were CP-7429 capillary column for TCD, and DB-5 capillary column for FID. CP-7429 column was composed of two parallel columns (CP-Molsieve 5Å and PoraBOND Q) which allowed us to detect

H_2, O_2, CO, CH_4, CO_2, C_2H_2, C_2H_4, C_2H_6, C_3H_6, and C_3H_8. By DB-5 column, CH_3OH and HCHO were identified. Methane conversion and methanol yield were obtained at ambient temperature. However, the reaction temperature was varied from room temperature to about 100 ºC depending on the plasma condition. Methane conversion, and selectivity and yield of CO, CO_2, and CH_3OH are obtained in the following:

$$\text{Conversion}(CH_4) = \frac{mol(consumed\ CH_4)}{mol(introduced\ CH_4)} \times 100[\%] \quad (12)$$

$$\text{Selectivity}(\text{CO}) = \frac{mol(produced\ CO)}{mol(converted\ CH_4)} \times 100[\%] \quad (13)$$

$$\text{Selectivity}(CO_2) = \frac{mol(produced\ CO_2)}{mol(converted\ CH_4)} \times 100[\%] \quad (14)$$

$$\text{Selectivity}(CH_3OH) = \frac{mol(produced\ CH_3OH)}{mol(converted\ CH_4)} \times 100[\%] \quad (15)$$

$$\text{Yield}(\text{Product}) = \frac{Conversion(CH_4) \times Selectivity(Product)}{100}[\%] \quad (16)$$

4.2.4. HO* analysis system

The OH radical was analyzed by HPLC (Agilent) equipped with a column of Shodex KC-811 maintained at 60 ºC. Phosphoric acid (5 mm) was used as a mobile phase at a flow rate of 1 ml/min. Variable wavelength (VW) detector was used in the HPLC system to confirm the quantification of water-soluble organic compounds such as salicylic acid, 2,5-dihydroxybenzoic acid (2,5-DHBA), 2,3-dihydroxybenzoic acid (2,3-DHBA) at 316 nm.

In order to collect HO* radical produced during the plasma reaction, a solution which was made by 0.02 g salicylic acid dissolving in 5 ml anhydrous ethanol was dripped equably onto the surface of the catalyst. After that, the catalyst was dried at

105 ºC. When salicylic acid reacts with OH radical, oxygenated products including 2,3-DHBA and 2,5-DHBA are produced. Since OH radical is more reactive than other chemicals, the products mainly comes from OH radical [115]. When the sampling time was too short, the conversion could not be calculated by HPLC due to small amount of the reacted salicylic acid. In addition, long sampling time could make the salicylic acid exhausted under plasma condition [116]. Therefore, the sampling time was maintained to 10 min. After the reaction, the catalyst was dipped in distilled water (10 ml) and dissolution of the products was carried out. The salicylic acid conversion was calculated by the following equations:

$$\text{Conversion(SA)} = \frac{mol(consumed\ SA)}{mol(introduced\ SA)} \times 100[\%] \quad (17)$$

Where SA represents salicylic acid.

4.3. Results and discussion

4.3.1. Direct methanol synthesis from methane under plasma only condition

Firstly, our experiment was conducted under plasma only condition in order to compare with the plasma-catalyst hybrid reaction. In plasma only reaction, methane conversion and methanol selectivity were measured in the range of plasma power from 6.5 kV_{P-P} to 8.5 kV_{P-P} at ambient temperature. Because of the plasma property, methane was able to activate and oxidize without the addition of any thermal energy. Oxygenated products except CO, CO_2, and methanol were hardly detected. Among the products, CO was the most abundant product during the reaction. The plasma power calculated from V-Q Lissajous figure changed from 2.3 W to 7.2 W (from 1.4 kJ/L to 4.3 kJ/L) depending on the input voltage which led to vary the reaction temperature from 61 ºC to 108 ºC. As the input voltage increased, methanol selectivity decreased in this period since the selectivity of more oxygenated products such as CO and CO_2 was enhanced. However, methane conversion also went up due to the increase of plasma power. Consequently, the overall methanol yield increased from 5.1% to 8.7% while input voltage varied from 6.5 kV_{P-P} to 8.5 kV_{P-P}. It was confirmed that methanol yield steadily increased although methanol selectivity got lower as the input voltage went up in this reaction condition. Under the plasma condition, oxygen radical, methyl radical, and hydrogen radical can be produced. According to Wang et al. [117], the possible reaction pathways for the formation of methanol under plasma condition are proposed as shown in Scheme 4-1.

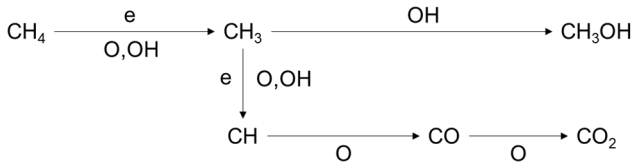

Scheme 4-1. Possible reaction pathways for the direct methanol synthesis from methane under plasma condition.

4.3.2. Glass bead effect on direct methanol synthesis under plasma condition

In order to improve the productivity of methanol, glass bead was loaded to the reactor as a packing material. Before the loading, the glass bead was etched by 5 M NaOH solution in order to enhance the adhesion of metal oxide. After the insertion of glass bead, the plasma configuration became much more stabilized as shown in Figure 4-3 due to the spherical shape and low dielectric constant of the glass bead. At all plasma conditions from 6.5 kV_{P-P} to 8.5 kV_{P-P} at ambient temperature, the reaction of glass bead with plasma showed higher methanol yield than plasma only reaction. The methanol yield increased from 6.3% to 9.6% in the presence of the glass bead. However, the methanol selectivity decreased as the input voltage got higher. It was confirmed that methanol yield did hardly increase above 7.5 kV_{P-P}. Furthermore, the increase rate, which is the division of methanol yield in the presence of glass bead by that of plasma only, decreased from 124.4% to 110.8%. The plasma power varied from 2.2 W to 7.6 W (from 1.3 kJ/L to 4.5 kJ/L) according to the input voltage, which was similar to plasma only reaction. Considering the reactivity and specific input energy, 7.5 kV_{P-P} was selected as the optimum plasma condition.

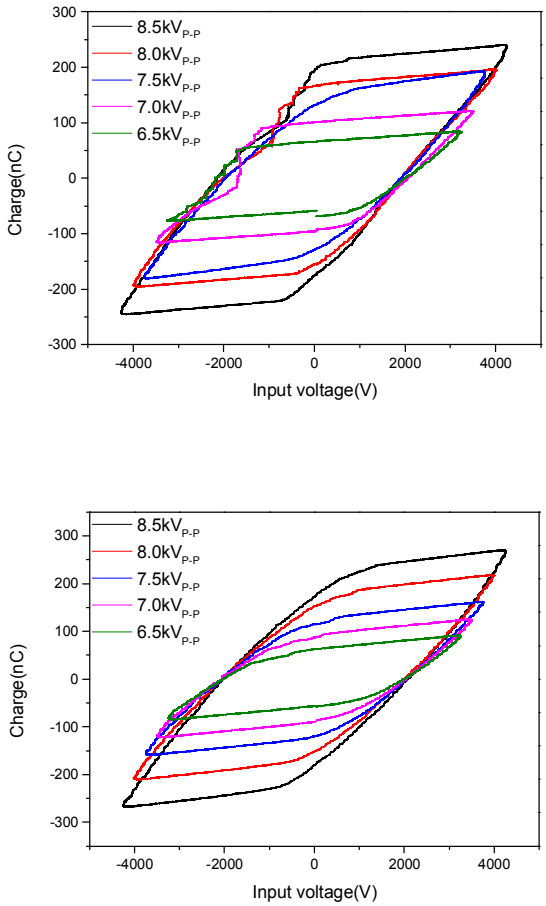

Figure 4-3. Lissajous figure of plasma only condition (top) and glass bead under plasma condition (bottom).

4.3.3. Metal oxide-coated glass bead for methanol synthesis with plasma

Glass bead showed synergistic effect with plasma for partial oxidation of methane to methanol. Therefore, the glass bead was selected as packing material. On the glass bead, some transition metal oxides such as MnO, Mn_2O_3, MnO_2, Fe_2O_3, NiO, and Co_3O_4 were coated to enhance the activity for methanol synthesis. The surface area of all catalysts were below 1 m^2/g. As displayed in Table 4-1, MnO, Mn_2O_3, and Fe_2O_3 showed the higher activity than glass bead with plasma.

The catalysts displayed similar plasma configuration and power to that of glass bead. Hence, it can be inferred that this synergistic effect did not come from plasma alteration but from catalytic reaction. On the other hand, MnO_2, NiO, and Co_3O_4 demonstrated poor activity, which was even lower than plasma only condition. In case of MnO_2, NiO, and Co_3O_4, the plasma configuration became conductive according to the Lissajous figure (Figure 4-4). Due to the increased conductivity, the plasma power dropped significantly and plasma was nearly extinguished, which gave rise to the sharp decrease of methane conversion. Among them, MnO_2 showed high methanol selectivity though it indicated low methane conversion since the plasma was hardly formed. After the reaction, all the catalysts did not seem to undergo severe alteration.

Long term activity of the catalyst was explored in order to confirm the durability of the catalyst and apply for practical application. Figure 4-5 shows the methane conversion, methanol selectivity, and methanol yield of Mn_2O_3/glass bead which showed the highest methanol yield in the plasma-catalyst hybrid system with time-on-stream (TOS). As shown in Figure 4-5, during the first one hour reaction, methane conversion increased and methanol selectivity decreased, which resulted in the slight increment of methanol yield. After the reaction for 10 h, the methanol

yield was stabilized at about 12%. This led to the fact that plasma-catalyst hybrid system is active and stable for direct methanol synthesis from methane.

It is known that the formation of OH radical is crucial for methanol synthesis from methane [118, 119]. According to Guo et al. [115], OH radical can be adsorbed well to MnO_x catalyst. Therefore, the amount of OH radical adsorbed on the catalyst was measured by HPLC. The analysis was conducted to the catalysts such as MnO, Mn_2O_3, and Fe_2O_3 which showed stable plasma configuration under the plasma condition. In order to estimate the amount of OH radical produced during the plasma reaction, a solution which was made by 0.02 g salicylic acid dissolving in 5 ml anhydrous ethanol was dripped equably onto the surface of the catalyst. After that, the catalyst was dried at 105 ºC. When salicylic acid reacts with OH radical on the surface of catalyst, 2,3-dihydroxybenzoic acid (2,3-DHBA), 2,5-dihydroxybenzoic acid (2,5-DHBA), and more oxygenated products such as CO and CO_2 are produced. Since OH radical is more reactive than other chemicals, the conversion of salicylic acid mainly comes from OH radical [115]. When the sampling time was too short, the conversion could not be calculated by HPLC due to small amount of the reacted salicylic acid. In addition, long sampling time could make the salicylic acid exhausted under plasma condition [116]. Therefore, the sampling time was maintained to 10 min. After the reaction, the catalyst was dipped in distilled water (10 ml) and dissolution of the products was carried out. As a result, Mn_2O_3 and MnO which showed high methanol yield exhibited low conversion of salicylic acid unlike what we expected.

The measured conversion of salicylic acid on MnO, Mn_2O_3, Fe_2O_3, and glass bead were 38.7%, 22.8%, 62.5%, and 65.5% respectively. Salicylic acid can be converted only when the OH radical reacts with salicylic acid. However, OH

radical can react with methane as well as salicylic acid to produce methanol in our study. Hence, it can be said that the amount of reacted salicylic acid does not have to be proportional to the adsorption quantity of OH radical.

The reaction of salicylic acid and OH radical can be a competitive reaction to methanol synthesis by methane and OH radical. Therefore, it can be inferred that less amount of salicylic acid is converted as the reaction selectivity of methane and OH radical is higher. Figure 4-6 indicates the correlation between the conversion of salicylic acid and the methanol yield, which leads to the result that the amount of converted salicylic acid is inversely proportional to the methanol yield. The OH radical reaction selectivity between salicylic acid and methane can be deduced from Table 4-2. According to Table 4-2, Mn_2O_3 shows the lowest ratio of salicylic acid conversion to methanol yield, which presents high OH radical reactivity to methane between salicylic acid and methane. Indeed, contrary to the Mn_2O_3-coated glass bead and MnO-coated glass bead, methanol yield decreased from 8.9% to 7.1% when the only glass bead with salicylic acid was loaded. This led to the fact that OH radical which was supposed to react with methane to generate methanol actually reacted with salicylic acid. From this result, it was confirmed that the manganese oxide could increase the reaction selectivity of methane and OH radical.

Table 4-1. Methane conversion and products selectivity of metal oxide-coated glass bead under plasma condition (7.5kV$_{P-P}$, 4kHz).

Samples[a]	Methane conversion (%)	Selectivity (%)			Methanol yield (%)
		CO	CO_2	Methanol	
P	23.3	49.6	15.0	32.6	7.6
GB+P	26.6	48.3	13.9	34.9	9.3
MnO/GB+P	33.1	48.4	13.7	34.4	11.4
Mn_2O_3/GB+P	30.5	43.8	13.6	40.2	12.3
MnO_2/GB+P	10.4	29.8	12.3	53.7	5.6
Fe_2O_3/GB+P	33.2	51.7	14.2	29.3	9.7
Co_3O_4/GB+P	13.1	34.4	24.3	31.5	4.1
NiO/GB+P	17.7	47.1	11.6	36.9	6.5
P[120][b]	41.0	41.5	19.5	19.5	8.0
Fe-HZSM-5[121][c]	31.5	-	72.1	10.8	3.4

[a] P and GB represent plasma and glass bead, respectively. [b] The specific input energy (SEI) is 30 kJ/L without catalyst at 50 ºC. [c] Temperature: 630 ºC, contact time: 2.5 s, oxygen: 15.5 vol%, Si/Fe ratio: 22, without plasma.

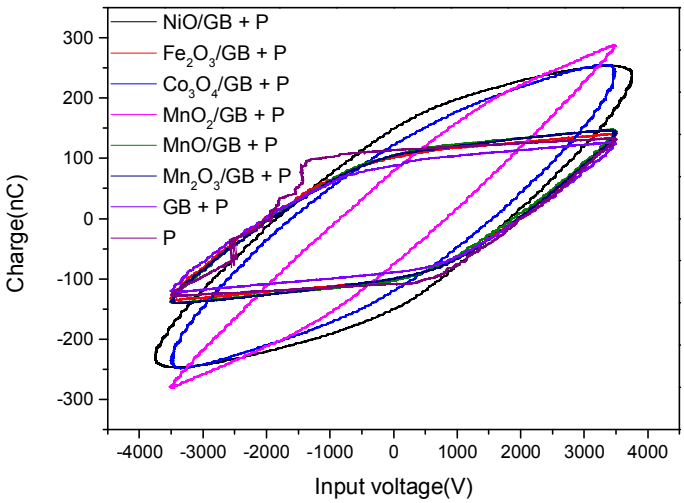

Figure 4-4. Lissajous figure of metal oxide-coated glass bead under plasma condition; GB=Glass bead, P=Plasma.

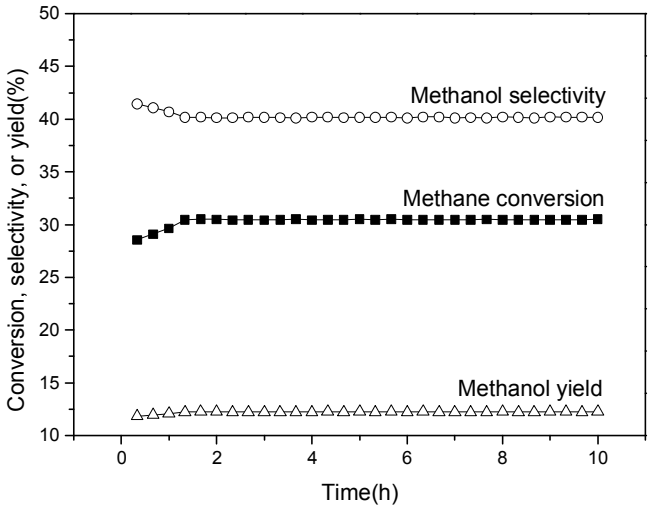

Figure 4-5. Conversion of methane, selectivity and yield of methanol over Mn_2O_3/glass bead as a function of time on stream.

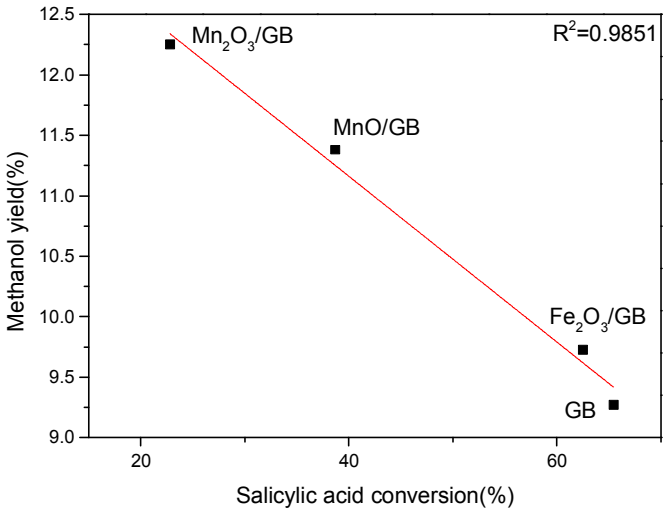

Figure 4-6. The correlation between amount of OH detected by HPLC and methanol yield; GB=Glass bead.

Table 4-2. Salicylic acid conversion, methanol yield, and their ratio of metal oxide-coated glass bead under plasma condition (7.5 kV_{P-P}, 4 kHz).

	Salicylic acid conversion[a](%)	Methanol yield[a](%)	**Salicylic acid conversion / Methanol yield**
GB+P	65.5	7.1	9.2
MnO/GB+P	38.7	10.8	3.6
Mn_2O_3/GB+P	22.8	11.7	2.0
Fe_2O_3/GB+P	62.5	8.6	7.2

[a] The salicylic acid conversion and methanol yield was measured after the 10 min reaction.

Chapter 5. Summary and Conclusions

In this work, plasma and non-PGM catalyst were combined to apply for methane complete oxidation. According to the previous literature, the hybridization of plasma and palladium-based catalyst was verified to be effective way to lower the light-off temperature of methane complete oxidation. In terms of methane conversion, non-PGM catalysts such as $CoCr_2O_4$ and $Co_1Ni_1O_x$ catalysts did not show much synergistic effect. However, CO selectivity dropped and CO_2 selectivity increased sharply while Co_1Ni_1Ox was loaded in plasma-catalyst hybrid system. Also, the methane oxidation ability did not affect the CO selectivity at hybrid condition since the $CoCr_2O_4$ which had the highest methane conversion showed the highest CO selectivity. At low temperature, insulating properties of material were more important than methane oxidation ability in the case of hybrid condition. Thus, catalysts mainly oxidized CO to CO_2 until the light-off temperature of each catalyst. Among the catalysts, $Co_1Ni_1O_x(500)$ presented the best performance under plasma-catalyst hybrid reaction. It was concluded that non-PGM catalysts with DBD plasma could have higher methane conversion than catalyst only condition and much lower CO selectivity than plasma only condition.

Combined reaction system of plasma and catalyst was applied to OCM reaction in order to lower the reaction temperature of OCM. Under plasma only condition, methane started to be activated and some hydrocarbons were produced at low temperature. Also, as temperature went up, methane conversion and C_{2+} hydrocarbon selectivity increased since more reactive species were generated due to the increase in plasma power. SiO_2 showed the best hydrocarbon yield among the various supports like $BaTiO_3$, TiO_2, γ-Al_2O_3, and SiO_2. Hence, diverse metals were loaded on SiO_2. Among various metals impregnated on SiO_2, Ag/SiO_2 catalyst

presented suitable performance with DBD plasma (9.7%) at 385 °C where common OCM reaction using catalytic process did not take place. Also, non-OCM reaction was conducted to investigate the effect of oxygen on the reactivity of OCM. Consequently, Ag/SiO_2 did not reveal much synergistic effect in the absence of oxygen, which meant oxygen played a key role with the catalyst.

The OCM reaction was carried out for 180 min to investigate the stability of plasma-catalyst hybrid system. As a result, the continuous deactivation was observed due to the formation of carbon deposition. Therefore, plasma and thermal regeneration were applied to regenerate the aged catalyst for OCM reaction. The plasma regeneration could recover the activity of the plasma-catalyst hybrid system at low temperature whereas the thermal regeneration could not. In addition, thermal regeneration influenced the textural property of the catalyst, which resulted in the decrease of the catalyst reactivity even after the regeneration process.

Plasma-catalyst hybrid system was applied to direct methanol synthesis from methane. Under plasma only condition, methane started to be activated to produce methanol below 100 ºC. By loading glass bead, plasma configuration became stabilized, which led to the increase of methanol yield. Some transition metal oxide such as MnO_x, Fe_2O_3, Co_3O_4, NiO were coated on the glass bead in order to enhance the activity. Among the catalysts, Mn_2O_3, MnO showed synergistic effect with plasma below 100 ºC, at ambient pressure in a continuous packed bed reactor. The amount of OH radical which was adsorbed on the catalyst was estimated from HPLC result. In this process, it was confirmed that the MnO_x catalyst could augment the reaction selectivity of methane and OH radical, which resulted in the formation of methanol. Furthermore, the stability of the catalyst was maintained for 10 h, presenting that the plasma-catalyst hybrid system could be an efficient

process for direct methanol synthesis from methane.

Bibliography

[1] N. Krichene, World crude oil and natural gas: a demand and supply model, Energy economics 2002;24:557-576.

[2] J.H. Lunsford, The Catalytic Oxidative Coupling of Methane, Angew. Chem. Int. Ed. 1995;34:970-980.

[3] Z. Li, G.B. Hoflund, A review on complete oxidation of methane at low temperatures, Journal of Natural Gas Chemistry 2003;12:153-160.

[4] J.-q. Zhang, Y.-j. Yang, J.-s. Zhang, Q. Liu, K.-r. Tan, Non-oxidative coupling of methane to C_2 hydrocarbons under above-atmospheric pressure using pulsed microwave plasma, Energy Fuels 2002;16:687-693.

[5] P. Cao, S. Adegbite, H. Zhao, E. Lester, T. Wu, Tuning dry reforming of methane for FT syntheses: A thermodynamic approach, Appl. Energy 2017;

[6] J.H. Park, D.W. Lee, S.W. Im, Y.H. Lee, D.J. Suh, K.W. Jun, K.Y. Lee, Oxidative coupling of methane using non-stoichiometric lead hydroxyapatite catalyst mixtures, Fuel 2012;94:433-439.

[7] F. Raouf, M. Taghizadeh, M. Yousefi, Activity enhancement of Li/MgO catalysts by lithium chloride as a lithium precursor for the oxidative coupling of methane, React. Kinet. Mech. Cat. 2013;110:373-385.

[8] L.B. Pierella, L. Wang, O.A. Anunziata, Methane direct conversion to aromatic hydrocarbons at low reaction temperature, React. Kinet. Catal. Lett. 1997;60:101-106.

[9] X. Guo, G. Fang, G. Li, H. Ma, H. Fan, L. Yu, C. Ma, X. Wu, D. Deng, M. Wei, Direct, nonoxidative conversion of methane to ethylene, aromatics, and hydrogen, Science 2014;344:616-619.

[10] S. Morejudo, R. Zanón, S. Escolástico, I. Yuste-Tirados, H. Malerød-Fjeld, P.

Vestre, W. Coors, A. Martínez, T. Norby, J. Serra, Direct conversion of methane to aromatics in a catalytic co-ionic membrane reactor, Science 2016;353:563-566.

[11] P. Tang, Q. Zhu, Z. Wu, D. Ma, Methane activation: the past and future, Energy & Environmental Science 2014;7:2580-2591.

[12] T. Baldwin, R. Burch, Catalytic combustion of methane over supported palladium catalysts: I. Alumina supported catalysts, Applied catalysis 1990;66:337-358.

[13] J.P. Van Hook, Methane-steam reforming, Catalysis Reviews—Science and Engineering 1980;21:1-51.

[14] V. Degirmenci, D. Uner, A. Yilmaz, Methane to higher hydrocarbons via halogenation, Catal. Today 2005;106:252-255.

[15] G. Suits, H. Salzberg, The collected works of Irving Langmuir, J. Electrochem. Soc. 1963;110:239C-240C.

[16] H. Conrads, M. Schmidt, Plasma generation and plasma sources, Plasma Sources Sci. Technol. 2000;9:441-454.

[17] T. Nozaki, K. Okazaki, Non-thermal plasma catalysis of methane: Principles, energy efficiency, and applications, Catal. Today 2013;211:29-38.

[18] D.H. Lee, Y.-H. Song, K.-T. Kim, J.-O. Lee, Comparative study of methane activation process by different plasma sources, Plasma Chem. Plasma Process. 2013;33:647-661.

[19] E. Gomez, D.A. Rani, C.R. Cheeseman, D. Deegan, M. Wise, A.R. Boccaccini, Thermal plasma technology for the treatment of wastes: a critical review, J. Hazard. Mater. 2009;161:614-626.

[20] T. Oda, Non-thermal plasma processing for environmental protection: decomposition of dilute VOCs in air, J. Electrostat. 2003;57:293-311.

[21] H.H. Kim, Nonthermal plasma processing for air□pollution control: a historical review, current issues, and future prospects, Plasma Process. Polym. 2004;1:91-110.

[22] U. Kogelschatz, Dielectric-barrier discharges: their history, discharge physics, and industrial applications, Plasma Chem. Plasma Process. 2003;23:1-46.

[23] W.S. Kang, D.H. Lee, J.-O. Lee, M. Hur, Y.-H. Song, Combination of plasma with a honeycomb-structured catalyst for automobile exhaust treatment, Environ. Sci. Technol. 2013;47:11358-11362.

[24] R. Marques, S. Da Costa, P. Da Costa, Plasma-assisted catalytic oxidation of methane: On the influence of plasma energy deposition and feed composition, Applied Catalysis B: Environmental 2008;82:50-57.

[25] T. Nozaki, N. Muto, S. Kado, K. Okazaki, Dissociation of vibrationally excited methane on Ni catalyst: Part 1. Application to methane steam reforming, Catal. Today 2004;89:57-65.

[26] S. Jo, T. Kim, D.H. Lee, W.S. Kang, Y.-H. Song, Effect of the electric conductivity of a catalyst on methane activation in a dielectric barrier discharge reactor, Plasma Chem. Plasma Process. 2014;34:175-186.

[27] J. Amouroux, S. Cavadias, A. Doubla, Carbon Dioxide reduction by non-equilibrium electrocatalysis plasma reactor, IOP Conference Series: Materials Science and Engineering, IOP Publishing, 2011, pp. 012005.

[28] T. Kim, S. Jo, Y.-H. Song, D.H. Lee, Synergetic mechanism of methanol–steam reforming reaction in a catalytic reactor with electric discharges, Appl. Energy 2014;113:1692-1699.

[29] J. Van Durme, J. Dewulf, C. Leys, H. Van Langenhove, Combining non-thermal plasma with heterogeneous catalysis in waste gas treatment: a review,

Applied Catalysis B: Environmental 2008;78:324-333.

[30] X.J. Wang, Q. Yang, C.G. Yao, X.X. Zhang, C.X. Sun, Dielectric Barrier Discharge Characteristics of Multineedle-to-Cylinder Configuration, Energies 2011;4:2133-2150.

[31] K. Takaki, Y. Hatanaka, K. Arima, S. Mukaigawa, T. Fujiwara, Influence of electrode configuration on ozone synthesis and microdischarge property in dielectric barrier discharge reactor, Vacuum 2008;83:128-132.

[32] P. Gélin, M. Primet, Complete oxidation of methane at low temperature over noble metal based catalysts: a review, Applied Catalysis B: Environmental 2002;39:1-37.

[33] O. Boucher, P. Friedlingstein, B. Collins, K.P. Shine, The indirect global warming potential and global temperature change potential due to methane oxidation, Environmental Research Letters 2009;4:044007.

[34] K.P. Shine, J.S. Fuglestvedt, K. Hailemariam, N. Stuber, Alternatives to the global warming potential for comparing climate impacts of emissions of greenhouse gases, Clim. Change 2005;68:281-302.

[35] P. Artizzu-Duart, Y. Brulle, F. Gaillard, E. Garbowski, N. Guilhaume, M. Primet, Catalytic combustion of methane over copper-and manganese-substituted barium hexaaluminates, Catal. Today 1999;54:181-190.

[36] L. Marchetti, L. Forni, Catalytic combustion of methane over perovskites, Applied Catalysis B: Environmental 1998;15:179-187.

[37] L. Lisi, G. Bagnasco, P. Ciambelli, S. De Rossi, P. Porta, G. Russo, M. Turco, Perovskite-type oxides: II. Redox properties of $LaMn_{1-x}Cu_xO_3$ and $LaCo_{1-x}Cu_xO_3$ and methane catalytic combustion, J. Solid State Chem. 1999;146:176-183.

[38] S. Nguyen, V. Szabo, D.T. On, S. Kaliaguine, Mesoporous silica supported

$LaCoO_3$ perovskites as catalysts for methane oxidation, Microporous Mesoporous Mater. 2002;54:51-61.

[39] S. Pengpanich, V. Meeyoo, T. Rirksomboon, K. Bunyakiat, Catalytic oxidation of methane over CeO_2-ZrO_2 mixed oxide solid solution catalysts prepared via urea hydrolysis, Applied Catalysis A: General 2002;234:221-233.

[40] V. Kharton, V. Sobyanin, V. Belyaev, G. Semin, S. Veniaminov, E. Tsipis, A. Yaremchenko, A. Valente, I. Marozau, J. Frade, Methane oxidation on the surface of mixed-conducting $La_{0.3}Sr_{0.7}Co_{0.8}Ga_{0.2}O_{3-\delta}$, Catal. Commun. 2004;5:311-316.

[41] L.-h. Xiao, K.-p. Sun, X.-l. Xu, X.-n. Li, Low-temperature catalytic combustion of methane over Pd/CeO_2 prepared by deposition–precipitation method, Catal. Commun. 2005;6:796-801.

[42] D.O. Simone, T. Kennelly, R.J. Farrauto, Reversible poisoning of palladium catalysts for methane oxidation, Applied catalysis 1991;70:87-100.

[43] C. Méthivier, J. Massardier, J. Bertolini, Pd/Si_3N_4 catalysts: preparation, characterization and catalytic activity for the methane oxidation, Applied Catalysis A: General 1999;182:337-344.

[44] K. Sekizawa, H. Widjaja, S. Maeda, Y. Ozawa, K. Eguchi, Low temperature oxidation of methane over Pd catalyst supported on metal oxides, Catal. Today 2000;59:69-74.

[45] K.-i. Muto, N. Katada, M. Niwa, Complete oxidation of methane on supported palladium catalyst: Support effect, Applied Catalysis A: General 1996;134:203-215.

[46] H.-H. Kim, Y. Teramoto, T. Sano, N. Negishi, A. Ogata, Effects of Si/Al ratio on the interaction of nonthermal plasma and Ag/HY catalysts, Applied Catalysis B: Environmental 2015;166:9-17.

[47] P. Bruggeman, N. Sadeghi, D. Schram, V. Linss, Gas temperature

determination from rotational lines in non-equilibrium plasmas: a review, Plasma Sources Sci. Technol. 2014;23:023001.

[48] G. Petitpas, J.-D. Rollier, A. Darmon, J. Gonzalez-Aguilar, R. Metkemeijer, L. Fulcheri, A comparative study of non-thermal plasma assisted reforming technologies, Int. J. Hydrogen Energy 2007;32:2848-2867.

[49] Y. Lee, J. Chung, Y. Choi, J. Chung, M. Cho, W. Namkung, NO_x removal characteristics in plasma plus catalyst hybrid process, Plasma Chem. Plasma Process. 2004;24:137-154.

[50] H. Lee, D.-H. Lee, Y.-H. Song, W.C. Choi, Y.-K. Park, D.H. Kim, Synergistic effect of non-thermal plasma–catalysis hybrid system on methane complete oxidation over Pd-based catalysts, Chem. Eng. J. 2015;259:761-770.

[51] J. Kriegseis, B. Möller, S. Grundmann, C. Tropea, Capacitance and power consumption quantification of dielectric barrier discharge (DBD) plasma actuators, J. Electrostat. 2011;69:302-312.

[52] J. Chen, X. Zhang, H. Arandiyan, Y. Peng, H. Chang, J. Li, Low temperature complete combustion of methane over cobalt chromium oxides catalysts, Catal. Today 2013;201:12-18.

[53] J. Chen, W. Shi, J. Li, Catalytic combustion of methane over cerium-doped cobalt chromite catalysts, Catal. Today 2011;175:216-222.

[54] S. Tanasoi, G. Mitran, N. Tanchoux, T. Cacciaguerra, F. Fajula, I. Săndulescu, D. Tichit, I.-C. Marcu, Transition metal-containing mixed oxides catalysts derived from LDH precursors for short-chain hydrocarbons oxidation, Applied Catalysis A: General 2011;395:78-86.

[55] Y.-F. Han, K. Ramesh, L. Chen, E. Widjaja, S. Chilukoti, F. Chen, Observation of the reversible phase-transformation of α-Mn_2O_3 nanocrystals during the catalytic

combustion of methane by in situ Raman spectroscopy, The Journal of Physical Chemistry C 2007;111:2830-2833.

[56] Y. Zhang, Z. Qin, G. Wang, H. Zhu, M. Dong, S. Li, Z. Wu, Z. Li, Z. Wu, J. Zhang, Catalytic performance of MnO_x–NiO composite oxide in lean methane combustion at low temperature, Applied Catalysis B: Environmental 2013;129:172-181.

[57] H. Kim, K. Takashima, S. Katsura, A. Mizuno, Low-temperature NO_x reduction processes using combined systems of pulsed corona discharge and catalysts, J. Phys. D: Appl. Phys. 2001;34:604.

[58] A.M. Harling, D.J. Glover, J.C. Whitehead, K. Zhang, The role of ozone in the plasma-catalytic destruction of environmental pollutants, Applied Catalysis B: Environmental 2009;90:157-161.

[59] M. Młotek, J. Sentek, K. Krawczyk, K. Schmidt-Szałowski, The hybrid plasma–catalytic process for non-oxidative methane coupling to ethylene and ethane, Applied Catalysis A: General 2009;366:232-241.

[60] A. Ogata, K. Yamanouchi, K. Mizuno, S. Kushiyama, T. Yamamoto, Decomposition of benzene using alumina-hybrid and catalyst-hybrid plasma reactors, IEEE Transactions on Industry Applications 1999;35:1289-1295.

[61] X. Tu, J.C. Whitehead, Plasma-catalytic dry reforming of methane in an atmospheric dielectric barrier discharge: Understanding the synergistic effect at low temperature, Appl. Catal. B: Environ. 2012;125:439-448.

[62] Z. Yu, X. Yang, J.H. Lunsford, M.P. Rosynek, Oxidative coupling of methane over Na_2WO_4/CeO_2 and related catalysts, J. Catal. 1995;154:163-173.

[63] B. Zohour, D. Noon, S. Senkan, Spatial Concentration and Temperature Profiles in Dual□Packed□Bed Catalytic Reactors: Oxidative Coupling of Methane,

ChemCatChem 2014;6:2815-2820.

[64] K. Aoki, M. Ohmae, T. Nanba, K. Takeishi, N. Azuma, A. Ueno, H. Ohfune, H. Hayashi, Y. Udagawa, Direct conversion of methane into methanol over MoO_3/SiO_2 catalyst in an excess amount of water vapor, Catal. Today 1998;45:29-33.

[65] L. Guczi, K.V. Sarma, L. Borko, Non-oxidative methane coupling over Co-Pt/NaY bimetallic catalysts, Catal. Lett. 1996;39:43-47.

[66] V. Choudhary, V. Rane, Acidity/basicity of rare-earth oxides and their catalytic activity in oxidative coupling of methane to C_2-hydrocarbons, J. Catal. 1991;130:411-422.

[67] J.W. Thybaut, J.J. Sun, L. Olivier, A.C. Van Veen, C. Mirodatos, G.B. Marin, Catalyst design based on microkinetic models: Oxidative coupling of methane, Catal. Today 2011;159:29-36.

[68] N.A.S. Amin, S.E. Pheng, Influence of process variables and optimization of ethylene yield in oxidative coupling of methane over Li/MgO catalyst, Chem. Eng. J. 2006;116:187-195.

[69] S. Arndt, T. Otremba, U. Simon, M. Yildiz, H. Schubert, R. Schomäcker, Mn–Na_2WO_4/SiO_2 as catalyst for the oxidative coupling of methane. What is really known?, Appl. Catal. A: Gen. 2012;425:53-61.

[70] U. Zavyalova, M. Geske, R. Horn, G. Weinberg, W. Frandsen, M. Schuster, R. Schlogl, Morphology and Microstructure of Li/MgO Catalysts for the Oxidative Coupling of Methane, Chemcatchem 2011;3:949-959.

[71] V. Salehoun, A. Khodadadi, Y. Mortazavi, A. Talebizadeh, Dynamics of $Mn/Na_2WO_4/SiO_2$ catalyst in oxidative coupling of methane, Chem. Eng. Sci. 2008;63:4910-4916.

[72] Y. Amenomiya, V.I. Birss, M. Goledzinowski, J. Galuszka, A.R. Sanger, Conversion of Methane by Oxidative Coupling, Cat. Rev. - Sci. Eng. 1990;32:163-227.

[73] B.L. Farrell, S. Linic, Oxidative coupling of methane over mixed oxide catalysts designed for solid oxide membrane reactors, Catal. Sci. Technol. 2016;6:4370-4376.

[74] T.W. Elkins, B.r. Neumann, M. Bäumer, H.E. Hagelin-Weaver, Effects of Li Doping on MgO-Supported Sm_2O_3 and TbOx Catalysts in the Oxidative Coupling of Methane, ACS Catal. 2014;4:1972-1990.

[75] S. Sadjadi, S. Jašo, H. Godini, S. Arndt, M. Wollgarten, R. Blume, O. Görke, R. Schomäcker, G. Wozny, U. Simon, Feasibility study of the Mn–Na_2WO_4/SiO_2 catalytic system for the oxidative coupling of methane in a fluidized-bed reactor, Catal. Sci. Technol. 2015;5:942-952.

[76] K. Oshima, K. Tanaka, T. Yabe, E. Kikuchi, Y. Sekine, Oxidative coupling of methane using carbon dioxide in an electric field over La–ZrO_2 catalyst at low external temperature, Fuel 2013;107:879-881.

[77] J.S. Lee, S. Oyama, Oxidative coupling of methane to higher hydrocarbons, Catalysis Reviews Science and Engineering 1988;30:249-280.

[78] E.V. Kondratenko, M. Baerns, Oxidative coupling of methane, 2008.

[79] W. Cho, Y. Baek, S.-K. Moon, Y.C. Kim, Oxidative coupling of methane with microwave and RF plasma catalytic reaction over transitional metals loaded on ZSM-5, Catal. Today 2002;74:207-223.

[80] C.E. Stere, W. Adress, R. Burch, S. Chansai, A. Goguet, W.G. Graham, F. De Rosa, V. Palma, C. Hardacre, Ambient Temperature Hydrocarbon Selective Catalytic Reduction of NO_x Using Atmospheric Pressure Nonthermal Plasma

Activation of a Ag/Al_2O_3 Catalyst, ACS Catal. 2014;4:666-673.

[81] P.G. Rutberg, V.A. Kuznetsov, V.E. Popov, S.D. Popov, A.V. Surov, D.I. Subbotin, A.N. Bratsev, Conversion of methane by CO_2+H_2O+CH_4 plasma, Appl. Energy 2015;148:159-168.

[82] Q.H. Trinh, Y.S. Mok, Environmental plasma-catalysis for the energy-efficient treatment of volatile organic compounds, Korean J. Chem. Eng. 2016;33:735-748.

[83] B. Eliasson, C.J. Liu, U. Kogelschatz, Direct conversion of methane and carbon dioxide to higher hydrocarbons using catalytic dielectric-barrier discharges with zeolites, Ind. Eng. Chem. Res. 2000;39:1221-1227.

[84] C.J. Liu, B.Z. Xue, B. Eliasson, F. He, Y. Li, G.H. Xu, Methane conversion to higher hydrocarbons in the presence of carbon dioxide using dielectric-barrier discharge plasmas, Plasma Chem. Plasma Process. 2001;21:301-310.

[85] X. Tu, H.J. Gallon, M.V. Twigg, P.A. Gorry, J.C. Whitehead, Dry reforming of methane over a Ni/Al_2O_3 catalyst in a coaxial dielectric barrier discharge reactor, J. Phys. D: Appl. Phys. 2011;44:274007.

[86] V. Goujard, J.-M. Tatibouët, C. Batiot-Dupeyrat, Use of a non-thermal plasma for the production of synthesis gas from biogas, Appl. Catal. A: Gen. 2009;353:228-235.

[87] Y. Yang, Direct non-oxidative methane conversion by non-thermal plasma: Experimental study, Plasma Chem. Plasma Process. 2003;23:283-296.

[88] A. Marafee, C.J. Liu, G.H. Xu, R. Mallinson, L. Lobban, An experimental study on the oxidative coupling of methane in a direct current corona discharge reactor over Sr/La_2O_3 catalyst, Ind. Eng. Chem. Res. 1997;36:632-637.

[89] H.K. Jeong, S.C. Kim, C. Han, H. Lee, H.K. Song, B.K. Na, Conversion of methane to higher hydrocarbons in pulsed DC barrier discharge at atmospheric

pressure, Korean J. Chem. Eng. 2001;18:196-201.

[90] F. Holzer, F.D. Kopinke, U. Roland, Influence of ferroelectric materials and catalysts on the performance of non-thermal plasma (NTP) for the removal of air pollutants, Plasma Chem. Plasma Process. 2005;25:595-611.

[91] R. Li, Q. Tang, S. Yin, T. Sato, Plasma catalysis for CO_2 decomposition by using different dielectric materials, Fuel Process. Technol. 2006;87:617-622.

[92] E.C. Neyts, K. Ostrikov, M.K. Sunkara, A. Bogaerts, Plasma Catalysis: Synergistic Effects at the Nanoscale, Chem. Rev. 2015;115:13408-13446.

[93] L. Wang, Y. Yi, Y. Zhao, R. Zhang, J. Zhang, H. Guo, NH_3 Decomposition for H_2 Generation: Effects of Cheap Metals and Supports on Plasma–Catalyst Synergy, ACS Catal. 2015;5:4167-4174.

[94] J. Robertson, High dielectric constant oxides, Eur. Phys. J. Appl. Phys. 2004;28:265-291.

[95] J. Robertson, High dielectric constant gate oxides for metal oxide Si transistors, Rep. Prog. Phys. 2005;69:327.

[96] M.M. Vijatovic, J.D. Bobic, B.D. Stojanovic, History and Challenges of Barium Titanate: Part II, Sci. Sinter. 2008;40:235-244.

[97] D. Mei, X. Zhu, Y.-L. He, J.D. Yan, X. Tu, Plasma-assisted conversion of CO_2 in a dielectric barrier discharge reactor: understanding the effect of packing materials, Plasma Sources Sci. Technol. 2014;24:015011.

[98] X.L. Zhang, C.S.M. Lee, D.M.P. Mingos, D.O. Hayward, Oxidative coupling of methane using microwave dielectric heating, Appl. Catal. A: Gen. 2003;249:151-164.

[99] S.L. Yao, F. Ouyang, A. Nakayama, E. Suzuki, N. Okumoto, A. Mizuno, Oxidative coupling and reforming of methane with carbon dioxide using a high-

frequency pulsed plasma, Energy Fuels 2000;14:910-914.

[100] J.-Q. Zhang, J.-S. Zhang, Y.-J. Yang, Q. Liu, Oxidative coupling and reforming of methane with carbon dioxide using a pulsed microwave plasma under atmospheric pressure, Energy Fuels 2003;17:54-59.

[101] X. Bao, M. Muhler, R. Schlogl, G. Ertl, Oxidative Coupling of Methane on Silver Catalysts, Catal. Lett. 1995;32:185-194.

[102] T.C. Rocha, A. Oestereich, D.V. Demidov, M. Havecker, S. Zafeiratos, G. Weinberg, V.I. Bukhtiyarov, A. Knop-Gericke, R. Schlogl, The silver-oxygen system in catalysis: new insights by near ambient pressure X-ray photoelectron spectroscopy, Phys. Chem. Chem. Phys. 2012;14:4554-4564.

[103] D.S. Su, T. Jacob, T.W. Hansen, D. Wang, R. Schlogl, B. Freitag, S. Kujawa, Surface chemistry of Ag particles: identification of oxide species by aberration-corrected TEM and by DFT calculations, Angew. Chem. Int. Ed. Engl. 2008;47:5005-5008.

[104] A.J. Nagy, G. Mestl, D. Herein, G. Weinberg, E. Kitzelmann, R. Schlögl, The correlation of subsurface oxygen diffusion with variations of silver morphology in the silver–oxygen system, J. Catal. 1999;182:417-429.

[105] A.J. Nagy, G. Mestl, R. Schlogl, The role of subsurface oxygen in the silver-catalyzed, oxidative coupling of methane, J. Catal. 1999;188:58-68.

[106] Y. Xu, J. Greeley, M. Mavrikakis, Effect of subsurface oxygen on the reactivity of the Ag(111) surface, J. Am. Chem. Soc. 2005;127:12823-12827.

[107] J.H. Lunsford, Catalytic conversion of methane to more useful chemicals and fuels: a challenge for the 21st century, Catal. Today 2000;63:165-174.

[108] R. Palkovits, M. Antonietti, P. Kuhn, A. Thomas, F. Schüth, Solid catalysts for the selective low□temperature oxidation of methane to methanol, Angew.

Chem. Int. Ed. 2009;48:6909-6912.

[109] Y. Wang, K. Otsuka, Catalytic oxidation of methane to methanol with H_2-O_2 gas mixture at atmospheric pressure, J. Catal. 1995;155:256-267.

[110] X. Gang, H. Birch, Y. Zhu, H.A. Hjuler, N.J. Bjerrum, Direct oxidation of methane to methanol by mercuric sulfate catalyst, J. Catal. 2000;196:287-292.

[111] R. Raja, P. Ratnasamy, Direct conversion of methane to methanol, Appl. Catal. A: Gen. 1997;158:L7-L15.

[112] C.N. Dixon, M.A. Abraham, Conversion of methane to methanol by catalytic supercritical water oxidation, J. Supercrit. Fluids 1992;5:269-273.

[113] M. Muehlhofer, T. Strassner, W.A. Herrmann, New catalyst systems for the catalytic conversion of methane into methanol, Angew. Chem. Int. Ed. 2002;41:1745-1747.

[114] K.-H. Wang, H.-H. Tsai, Y.-H. Hsieh, The kinetics of photocatalytic degradation of trichloroethylene in gas phase over TiO_2 supported on glass bead, Appl. Catal. B: Environ. 1998;17:313-320.

[115] Y. Guo, X. Liao, J. He, W. Ou, D. Ye, Effect of manganese oxide catalyst on the dielectric barrier discharge decomposition of toluene, Catal. Today 2010;153:176-183.

[116] G. Yufang, L. Xiaobin, Y. Daiqi, Detection of hydroxyl radical in plasma reaction on toluene removal, J. Environ. Sci. 2008;20:1429-1432.

[117] L. Wang, Y. Yi, C. Wu, H. Guo, X. Tu, One□Step Reforming of CO_2 and CH_4 into High□Value Liquid Chemicals and Fuels at Room Temperature by Plasma□Driven Catalysis, Angew. Chem. Int. Ed. 2017;56:13679-13683.

[118] C. Taylor, R. Noceti, New developments in the photocatalytic conversion of methane to methanol, Catal. Today 2000;55:259-267.

[119] M. Gondal, A. Hameed, Z. Yamani, A. Arfaj, Photocatalytic transformation of methane into methanol under UV laser irradiation over WO_3, TiO_2 and NiO catalysts, Chem. Phys. Lett. 2004;392:372-377.

[120] T. Nozaki, A. Hattori, K. Okazaki, Partial oxidation of methane using a microscale non-equilibrium plasma reactor, Catal. Today 2004;98:607-616.

[121] B. Michalkiewicz, Partial oxidation of methane to formaldehyde and methanol using molecular oxygen over Fe-ZSM-5, Appl. Catal. A: Gen. 2004;277:147-153.

국 문 초 록

천연가스는 전세계에 널리 퍼져있는 가장 풍부한 화석연료 중 하나이다. 천연가스는 다른 화석연료들에 비해 청정한 에너지원으로 알려져 있기 때문에 에너지원으로서 주목을 받고 있다. 이러한 장점에도 불구하고, 천연가스의 주요성분인 메탄이 지구온난화에 중요한 부분을 차지하고 있기 때문에 불연소된 천연가스의 배출이 문제가 되고 있다. 메탄은 이산화탄소에 비해 같은 양 대비 25–34배의 지구온난화 효과를 보이고, 긴 수명을 갖고 있다. 그러므로, 메탄의 완전 산화 반응은 지구온난화 같은 환경 문제에 대한 걱정을 하지 않고 메탄을 사용하기 위해 반드시 해결해야 할 문제이다. 연료로서의 역할을 제외하고, 메탄의 사용은 대부분 간접적인 방법인. 합성 가스를 통한 액상 탄화수소나 다른 화학제품들의 생산에 국한되어 왔다. 이러한 간접적인 방법은 흡열반응과 발열반응 사이를 왔다갔다하기 때문에 높은 운영비용과 낮은 열역학적 효율이라는 단점들을 가지고 있다. 그러므로, 메탄이 석유에 대안이 될 수 있는 원료로 직접 사용이 될 수 있다면 경제적인 관점에서 굉장히 바람직할 것이다. 따라서, 다양한 촉매를 이용하여 수십년 동안 메탄으로부터 올레핀, 방향족 탄화수소, 알코올과 같은 좀 더 가치가 높은 물질들로의 직접 전환에 대해 많은 노력이 있었다. 그러나 메탄은 안정한 탄소–수소 결합 때문에 활성화되기가 쉽지 않아서 메탄 완전 산화 반응이나 메탄으로부터 고부가가치 물질 생산과 같은 촉매 반응을 시작하기 위해 필요한 높은 온도와 압력과 같은 혹독한 반응 조건이 필요하다. 메탄의 활성화는 이러한 반응들을 시작하는 데에 있어서

굉장히 중요하다. 이러한 어려움을 극복하기 위해 다양한 촉매들을 연구하고 적용하였다. 그럼에도 불구하고, 메탄의 활성화 반응은 혹독한 반응 조건이 촉매를 비활성화시킬 수 있기 때문에 수행하기 어렵다. 메탄을 저온에서 활성화시킬 수 있는 대안은 플라즈마를 사용하는 것이다. 유전체 장벽 방전, 코로나, 아크, 스파크, 마이크로웨이브, 글로우 방전, 펄스 방전과 같은 다양한 열 플라즈마와 저온 플라즈마가 존재한다. 저온 플라즈마에서는, 높은 에너지를 갖는 전자들이 생성되고 이러한 전자들에 의해 다른 다양한 라디칼들이 생성될 수 있다. 전자의 무게는 매우 가볍기 때문에, 저온 플라즈마에서 기체 온도는 크게 상승하지 않는다. 본 연구에서는 유전체 장벽 방전 플라즈마가 다른 저온 플라즈마들에 비해 설치하기가 쉽기 때문에 유전체 장벽 방전 플라즈마를 사용하였다.

먼저, 촉매와 플라즈마가 하나의 시스템으로 융합되는 유전체 장벽 방전 플라즈마 쿼츠 튜브 반응기에서 메탄의 완전 산화 반응을 수행하였다. 코발트 니켈 산화물이나 코발트 크롬 산화물과 같은 비귀금속 촉매를 산화 촉매로 사용하였다. 플라즈마-촉매 반응기에 가해지는 인가 전압은 플라즈마-촉매 상호작용에 미치는 플라즈마 파워의 영향을 최소화하기 위해 4 kV_{P-P}로 고정하였다. 플라즈마만의 반응에서, 메탄은 상온에서부터 일산화탄소와 이산화탄소로 산화되기 시작하였고, 메탄 전환율은 온도가 상승함에 따라 활성 라디칼들이 더 많이 생성되면서 증가하였다. 그러나 플라즈마만의 반응에서는 200 ℃ 미만의 저온에서는 이산화탄소 이외에 다량의 일산화탄소가 생성되었다.

한편, 플라즈마-촉매 반응에서는 코발트 니켈 산화물과 같은 비귀금속 촉매 조건에서 메탄은 저온에서부터 대부분 이산화탄소로 산화되었다. 이를 통해, 촉매의 도움으로 완전 산화 반응이 성공적으로 수행됨을 알 수 있었다. 플라즈마는 메탄을 산화시켜 일산화탄소를 생성하는 역할을 하고, 저온에서 촉매가 이 일산화탄소를 이산화탄소로 완전 산화시키는 역할을 하는 것을 알 수 있었다. 따라서, 메탄 완전 산화 반응이 낮은 일산화탄소 선택성을 유지하면서 귀금속 촉매와 유사하게 기존의 비귀금속 촉매 반응에 비해 매우 낮은 온도에서 진행할 수 있었다.

다음으로, 플라즈마-촉매 융합 시스템을 이용하여 메탄으로 C_2, C_3 탄화수소를 생성하는 메탄 산화이량화 반응을 진행하였다. 기존의 촉매 반응은 700 ℃ 이상의 고온을 필요로 하기 때문에 반응 온도를 낮추기 위해 유전체 장벽 방전 플라즈마를 적용하였다. 우선, 저온에서 플라즈마-촉매 융합 반응에 적합한 지지체를 찾고자 하였다. 다양한 지지체들 중, 실리카(SiO_2)가 유전체 장벽 방전 플라즈마 조건에서 가장 높은 수율을 보였다. 다양한 금속들을 실리카에 담지하였고, 그 결과 Ag/SiO_2 촉매가 400 ℃ 미만에서 가장 높은 10% 정도의 C_{2+} 탄화수소 수율을 보였다. 이 과정에서 산소가, 촉매에서 메탄이 C_{2+} 탄화수소로 커플링되는 반응에 중요한 역할을 한다는 것을 증명하였다. 하지만 Ag/SiO_2 촉매는 플라즈마 조건에서 시간이 지남에 따라 코킹에 의해 비활성화가 진행되었다. 따라서, 메탄 산화이량화 반응 후에 재생 절차를 진행하였다. 그 결과, 부분적인 코킹 제거와 은의 소결로 인해 열 재생은 반응성을 완전히 회복시키지 못하였으나, 378 ℃에서

플라즈마 재생을 통해서 반응성을 완전히 회복할 수 있었다.

마지막으로, 플라즈마-촉매 융합 시스템에서 메탄으로부터의 메탄올 직접 생산을 수행하였다. 촉매만의 반응에서는 높은 압력과 배치 반응기를 필요로 하여, 이러한 어려움을 극복하기 위해 유전체 장벽 방전 플라즈마를 적용하였다. 전이금속 산화물 중에서, Mn_2O_3가 코팅된 유리 비드가 플라즈마-촉매 융합 시스템에서 약 12.3%로 가장 높은 메탄올 수율을 보였다. 반응 온도는 낮은 플라즈마 파워로 인해 100 ℃ 미만을 유지하였다. 또한, 이 촉매의 반응성은 10시간 동안 선택성의 변화없이 유지되었다. 메커니즘 연구를 통해, 플라즈마로 인해 전이 금속 산화물 촉매에 생성된 OH 라디칼이 메탄올 생성을 위해 메탄에 대한 높은 선택성을 갖는다는 것을 확인하였다.

주요어: 메탄 활성화 반응, 플라즈마-촉매 융합 시스템, 유전체 장벽 방전, 저온 반응

학번: 2014-30264